LAWRENCE
LIVERMORE
NATIONAL
LABORATORY

UCRL-JRNL-215066

Identification of isotopically primitive interplanetary dust particles: A NanoSIMS isotopic imaging study

C. Floss, F. J. Stadermann, J. P. Bradley, Z. R. Dai, S. Bajt, G. Graham, A. S. Lea

September 6, 2005

Geochimica et Cosmochimica Acta

Identification of Isotopically Primitive Interplanetary Dust Particles: A NanoSIMS Isotopic Imaging Study

Christine Floss[1], Frank J. Stadermann[1], John P. Bradley[2], Zu Rong Dai[2], Sasa Bajt[2], Giles Graham[2] and A. Scott Lea[3]

[1]Laboratory for Space Sciences, Washington University, St. Louis, MO 63130, USA

[2]Institute for Geophysics and Planetary Physics, Lawrence Livermore National Laboratory, Livermore, CA 94550, USA

[3]Pacific Northwest National Laboratory, Richland WA 99352, USA

for submission to

Geochimica et Cosmochimica Acta

July 2005

ABSTRACT

We have carried out a comprehensive survey of the isotopic compositions (H, B, C, N, O, S) of a suite of interplanetary dust particles (IDPs), including both cluster and individual particles. Isotopic imaging with the NanoSIMS shows the presence of numerous discrete hotspots that are strongly enriched in ^{15}N, including the largest ^{15}N enrichments (~1300 ‰) observed in IDPs to date. A number of the IDPs also contain larger regions with more modest enrichments in ^{15}N, leading to average bulk N isotopic compositions that are ^{15}N-enriched in these IDPs. Although C isotopic compositions are normal in most of the IDPs, two ^{15}N-rich hotspots have correlated ^{13}C anomalies. CN^-/C^- ratios suggest that most of the ^{15}N-rich hotspots are associated with relatively N-poor carbonaceous matter, although specific carriers have not been determined. H isotopic distributions are similar to those of N: D anomalies are present both as distinct very D-rich hotspots and as larger regions with more modest enrichments. Nevertheless, H and N isotopic anomalies are not directly correlated, consistent with results from previous studies.

Oxygen isotopic imaging shows the presence of abundant presolar silicate grains in the IDPs. The O isotopic compositions of the grains are similar to those found in presolar oxide and silicate grains from primitive meteorites. Most of the silicate grains in the IDPs have isotopic ratios consistent with meteoritic Group 1 oxide grains, indicating origins in oxygen-rich red giant and asymptotic giant branch stars, but several presolar silicates exhibit the ^{17}O and ^{18}O enrichments of Group 4 oxide grains, whose origin is less well understood.

Based on their N isotopic compositions, the IDPs studied here can be divided into two groups. One group is characterized as being "isotopically primitive" and consists of those IDPs that have anomalous bulk N isotopic compositions. These particles typically also contain numerous ^{15}N-rich hotspots, occasional C isotopic anomalies, and abundant presolar silicate grains. In contrast, the other "isotopically normal" IDPs have normal bulk N isotopic compositions and, although some contain ^{15}N-rich hotspots, none exhibit C isotopic anomalies and none contain presolar silicate or oxide grains. Thus, isotopically interesting IDPs can be identified and selected on the basis of their N isotopic compositions for further study. However, this distinction does not extend to H isotopic compositions. Although both H and N anomalies

are frequently attributed to the survival of molecular cloud material in IDPs and, thus, should be more common in IDPs with anomalous bulk N compositions, D anomalies are as common in normal IDPs as they are in those characterized as isotopically primitive, based on their N isotopes. This may be due to different effects of secondary processing on the isotopic systems involved.

1. INTRODUCTION

Interplanetary dust particles (IDPs) have been collected by NASA in the Earth's stratosphere since 1974 (Brownlee et al., 1976). These particles originate largely from comets and asteroids and are complex assemblages of various primitive solar system materials (e.g., Bradley, 2004). IDPs can be loosely divided into two morphological types, chondritic porous (CP) and chondritic smooth (CS). Chondritic porous IDPs are dominated by anhydrous minerals, including forsterite, enstatite, GEMS (glass with embedded metal and sulfides; Bradley, 1994), Fe-sulfides and carbonaceous matter. In contrast, chondritic smooth IDPs are composed predominantly of hydrated layer lattice silicates, together with carbonates, sulfides and some anhydrous crystalline silicates. While specific parent bodies are not known, hydrated IDPs have been linked to asteroidal sources (Bradley and Brownlee, 1992; Keller et al., 1992; Rietmeijer, 1992), whereas anhydrous IDPs may be more likely to have a cometary origin (Brownlee et al., 1995).

Isotopic measurements of IDPs show the presence of abundant extrasolar phases. Significant depletions and enrichments in H isotopic compositions have been found in IDPs (Zinner et al., 1983; McKeegan et al., 1985) and almost certainly have an interstellar origin. In addition to the fact that deuterium (D) is readily consumed during nucleosynthesis in stars, direct observation of hydrogen isotopic fractionation in cold molecular clouds (Millar et al., 1989) shows that D/H ratios of simple molecules are on the order of 10^{-1} to 10^{-2}; the D/H ratios of some IDPs approach these values (Messenger, 2000), suggesting the intact survival of interstellar molecules in some IDPs. Nitrogen isotopic anomalies are also common in IDPs (Stadermann et al., 1989; Stadermann, 1991; Messenger et al., 2003a) generally occurring as enrichments of ^{15}N. The origin of N isotopic anomalies is more complicated than that of hydrogen, because N isotopic fractionation has not been observed in the interstellar medium, and because anomalous N can also have a nucleosynthetic origin. However, recent theoretical work shows that chemical reactions in dense molecular clouds can produce elevated $^{15}N/^{14}N$ ratios (Terzieva and Herbst, 2000; Charnley and Rodgers, 2002).

Specific carrier phases have been difficult to identify due to the small size of IDPs, but carbonaceous matter appears to carry many of the H and N isotopic anomalies in IDPs

(McKeegan et al., 1985; Aléon et al., 2001, 2003; Keller et al., 2004). The lack of abundant isotopic anomalies in C has, thus, been one of the major puzzles in IDP research. Recently, the waters of hydration have also been implicated as a carrier of heavy hydrogen in two IDPs (Mukhopadhyay and Nittler, 2003).

The advent of the NanoSIMS, a new type of ion microprobe with the ability to make isotopic measurements at a sub-micron scale, has provided renewed opportunities to investigate the isotopic compositions of IDPs. Recent discoveries include the presence of presolar (circumstellar) silicate grains in IDPs (Messenger et al., 2003b) and the first observation of a C isotopic anomaly, in the form of a ^{13}C depletion associated with a ^{15}N enrichment, in an anhydrous IDP (Floss et al., 2004). In this study we report on the results of a comprehensive survey of carbon, nitrogen and oxygen isotopic measurements on a suite of IDPs using the NanoSIMS; we have also investigated other isotopic systems (H, B, S) in a subset of these IDPs. Our goal has been to gain a better understanding of the abundance, nature and distribution of isotopically anomalous phases in IDPs and thereby constrain both the nature of these phases and the parent bodies from which IDPs originate. Preliminary results have been reported by Floss and Stadermann (2002, 2003, 2004, 2005a).

2. EXPERIMENTAL

2.1 Sample preparation and documentation

The IDPs studied here consist of both cluster IDPs (large fragile particles that fragment upon impact onto the collector flag) and individual, or non-cluster, IDPs obtained from the Cosmic Dust Curatorial Facility at Johnson Space Center. Particles were dry-picked from the collector flags at JSC and were sent to Washington University on dimpled glass slides. A tungsten needle was used to transfer the particles from the slides to high-purity Au foils, into which they were subsequently pressed using spectroscopic grade quartz disks, together with appropriate isotopic standards for ion microprobe analysis. The particles were examined with a JEOL 840A scanning electron microscope (SEM) prior to ion microprobe analysis. High magnification secondary electron (SE) and backscattered electron (BSE) images were obtained for each IDP, and energy dispersive x-ray (EDX) spectra were taken by rastering over the area of the IDP in order to obtain bulk compositional information about each particle. In addition, high

magnification images were obtained of seven grains with anomalous oxygen isotopic compositions, using a Hitachi S-4500 field emission SEM. We also took EDX spectra of these grains using a 5 keV accelerating voltage to minimize contributions from underlying or surrounding material. Table 1 lists the particle designations (collector and particle index), nicknames used in this study (note that different fragments of the same cluster particles each have their own nickname), SEM characterizations and the suite of isotopic measurements carried out on each particle.

2.2 SIMS measurements

2.2.1 Hydrogen isotopes–ims 3f

Hydrogen isotopes were measured on a subset of IDPs with the Cameca ims3f at Washington University, using procedures similar to those described by McKeegan et al. (1985). Negative secondary H and D ions were measured at low mass resolution using a Cs^+ primary beam with a beam current of 1-2 nA. The beam was centered on the particle and slightly defocused; a field aperture was used to restrict secondary ion transmission to a 15–20 μm area, thereby reducing the contribution from background hydrogen. Measurements were made in automated peak jumping mode and typically consisted of 20 cycles through the two masses. Peak positions were centered on the exit slit of the mass spectrometer at the start of each measurement and were re-centered every 5 cycles throughout the measurement. Terrestrial amphibole grains ("WU amphibole"; D/H = 0.00014532; McKeegan, 1987) on the same sample mounts were measured along with the IDPs as isotopic standards to correct for instrumental mass fractionation. All H isotopic compositions are reported relative to SMOW (Standard Mean Ocean Water; D/H = 0.00015576; Lodders and Fegley, 1998).

2.2.2 Carbon and nitrogen isotopes–NanoSIMS

Carbon and nitrogen isotopes were measured simultaneously in raster imaging mode with the Washington University NanoSIMS. A ~2 pA 16 keV Cs^+ beam (~100 nm in diameter) was scanned over sample surface areas ranging in size from 5 x 5 μm^2 to 50 x 50 μm^2 depending on the size of the particle being analyzed (most areas were either 20 x 20 μm^2 or 25 x 25 μm^2). Secondary ions ($^{12}C^-$, $^{13}C^-$, $^{12}C^{14}N^-$, $^{12}C^{15}N^-$ and $^{28}Si^-$) were collected simultaneously in five electron multipliers at a mass resolution (m/Δm ~6500) sufficient to resolve interferences from

neighboring peaks (primarily $^{10}B^{16}O^-$ and $^{11}B^{16}O^-$ peaks from $^{12}C^{14}N^-$ and $^{12}C^{15}N^-$, respectively). Secondary electron images of the particles were also acquired during each analysis. Prior to each measurement the analysis area was sputter-cleaned for five minutes with a rastered high-current Cs^+ beam to implant Cs and remove surface contaminants. Each isotopic imaging measurement consisted of between 10 to 40 scans that were subsequently added together to constitute a single image measurement of either 256^2 or 512^2 pixels. This procedure allows for correction of image shifts during the analysis and allows observed isotopic anomalies to be verified through the different layers. The data were processed using custom software developed in our laboratory. Images were corrected for sample drift from layer to layer and were checked for statistical outliers. Instrumental mass fractionation is estimated to be not more than 1% for these measurements. 1-hydroxy benzotriazole hydrate was used as a standard for both C and N measurements ($^{12}C/^{13}C$ = 90, $^{14}N/^{15}N$ = 272) and isotopic ratios and errors were calculated following standard conventions. Compositions are considered anomalous if they deviate from normal by 3σ or more. Results are expressed as isotopic ratios and in δ notation, representing the deviation of the measured isotopic ratio from the terrestrial standard in parts per thousand (‰). Additional details about isotopic imaging measurements with the NanoSIMS can be found in Stadermann et al. (2005a).

2.2.3 Oxygen isotopes–NanoSIMS

Oxygen isotopic imaging was carried out to search for isotopically anomalous circumstellar grains. The procedures are similar to those described above for C and N, with the measured species being $^{16}O^-$, $^{17}O^-$, $^{18}O^-$ and $^{28}Si^-$ as well as $^{24}Mg^{16}O^-$ to distinguish silicates from non-silicate grains. Particular care was taken to ensure the complete separation of the $^{17}O^-$ peak from the isobaric $^{16}OH^-$ peak at high mass resolution. It should be noted, however, that the $^{24}Mg^{16}O^-$ peak cannot be separated from the adjacent $^{28}Si^{12}C^-$ peak, which may be significant in parts of the IDPs with high abundances of mixed organics and silicates. Because the bulk oxygen isotopic compositions of IDPs are solar within about 5% (Stadermann, 1991), the average oxygen isotopic composition of each IDP analyzed was normalized to the standard solar oxygen ratios ($^{16}O/^{17}O$ = 2625, $^{16}O/^{18}O$ = 499). Sub-grains in the IDPs are considered anomalous if their oxygen isotopic compositions deviate by more than 3σ from the range of compositions of all normal sub-grains within an analyzed IDP.

2.2.4 Sulfur isotopes–NanoSIMS

Sulfur isotopic compositions were measured using procedures similar to those described for C and N. The measured species were $^{12}C^-$, $^{28}Si^-$, $^{32}S^-$, $^{33}S^-$ and $^{34}S^-$; ^{36}S was not measured. Analogous to the oxygen isotopic measurements, it was assumed that bulk IDPs have solar sulfur isotopic compositions and, thus, the average sulfur isotopic composition of each area analyzed was normalized to the standard solar sulfur ratios ($^{32}S/^{33}S = 127$, $^{32}S/^{34}S = 22.6$).

2.2.4 Hydrogen and boron isotopes–NanoSIMS

Hydrogen and boron isotopes were measured simultaneously ($^1H^-$, $^2H^-$, $^{10}B^-$, $^{11}B^-$) using procedures similar to those described for C and N. However, because of the low abundances expected for D, the experimental conditions for these measurements were optimized to provide the maximum secondary signal (e.g., the use of a 750 μm beam limiting aperture, rather than the 150 μm aperture normally used). The higher primary beam current resulted in a larger primary beam diameter of ~250 nm at the sample, and a consequent degradation of the spatial resolution. As for the ims 3f H isotopic measurements, WU amphibole was used as a standard and all H isotopic compositions are reported relative to SMOW. Boron isotopes were assumed to have solar isotopic ratios in the bulk IDPs and, thus, the average boron isotopic composition of each area analyzed was normalized to the standard solar boron ratio ($^{11}B/^{10}B = 4$).

2.3 Transmission electron microprobe (TEM) measurements

Thin sections (~100 nm) of several IDPs were produced using an FEI Company DB237 dual beam Strata focused ion beam (FIB)/ FESEM microscopy. FIB is now widely used in both materials and geological sciences to prepare site-specific thin sections for TEM analysis (Heaney et al., 2001; Giannuzzi et al., 2004). The methodology is summarized as follows: the identified presolar grain within the IDP and the immediate surrounding area are coated with a film of Pt deposited initially using the electron beam and then the ion beam. The Pt films cap the region of interest (ROI) and protect it from excessive ion etching and ion beam induced damage during the precision milling. The Ga^+ ion beam operating at 5000 pA and 30 kV are used to ablate material on either side of the ROI, resulting in a 1 μm thick thin section. The ion beam operating at 1000 pA and 30 kV is then used to make under and side cuts into the section to enable extraction from

the bulk material using an in situ Omniprobe™ needle. For the extraction the needle is placed in contact with the edge of the section, the FIB is then used to deposit a Pt weld. After extraction from the bulk material the section moved over to a half-cut TEM grid. The FIB is used to weld the side of the section that is not attached to the needle to the edge of the grid, after which the contact with the needle is broken again using the FIB. The section is then subjected to further ion milling using beam currents from 300 pA to 100 pA at 30 kV. This repeated process results in a section that is approximately 100 nm thick.

The TEM sections were examined using 200 and 300 keV field emission transmission electron microscopes (Phillips CM 200 and CM 300 series). Bright-field and dark-field imaging, electron diffraction, lattice-fringe imaging, energy-dispersive X-ray spectroscopy and electron energy-loss spectroscopy were employed to investigate compositions, mineralogy and petrography. The sections were also compositionally mapped for C, N, O, Mg, Al, Si, S, Fe and Ni using x-ray mapping, and energy-filtered imaging for C, N, O and Fe. Both methods provide compositional images with ~2 nm spatial resolution. All images were recorded using a slow-scan charge-coupled-device (CCD) camera (1024 x 1024 pixels).

2.4 Scanning Auger spectrometer measurements

We used the PHI 680 Scanning Auger Microprobe located at Pacific Northwest National Laboratory (PNNL) to make Auger elemental image maps of several IDP areas containing isotopically anomalous phases. A detailed introduction to Auger spectroscopy is given by Watts and Wolstenholme (2003). Areas ranging in size from 6 x 8 μm^2 to 9 x 12 μm^2 were scanned using a 10 nA field-emission electron beam (with an estimated diameter of ~20 nm) at an accelerating voltage of either 10 or 20 kV. Secondary electrons and element-specific Auger electrons (C, Si, O, Mg, S, Fe, Ca, N, Al) were collected sequentially to produce elemental (128^2 or 256^2 pixels) and SE images (512^2 pixels) of the areas selected. Measurement times varied depending on the size of the images and the number of elements mapped, but were on the order of 5 to 10 hours.

3. RESULTS

3.1 Sample descriptions

We studied a total of 42 IDPs from NASA collector flags L2009, L2011 and L2036 (Table 1). Thirteen are individual IDPs, while the remaining 29 are fragments of cluster IDPs that broke apart upon impact with the collector surface; 14 different clusters are represented by these 29 particles. All of the particles studied here have compositions that are c-type according to the definition of Stadermann (1991). The EDX spectra of such particles contain Si, Mg, Fe and Al; the dominant element is either Si, Mg or Fe and the Al peak is less than that of either Mg or Si. Sulfur is not taken into account in this definition and we have therefore designated as S-rich those particles in which S is the dominant peak in the EDX spectrum. The spectra of some particles resemble those of single mineral compositions and are designated as such in Table 1; these IDPs may be dominated by either pyroxene or olivine, as indicated. Figure 1 shows examples of the four different IDP types and their corresponding spectra. IDP Rolland (Fig. 1a) is an individual IDP with a typical aggregate texture and c-type composition. Bunin (Fig. 1b) is part of a cluster IDP from collector L2036. Texturally it is similar to Rolland, but its EDX spectrum shows that it is dominated by FeS. Mommsen (Fig. 1c) is also part of a cluster IDP (from collector L2009). Its EDX spectrum is similar to that of a low-Ca pyroxene and much of the particle appears massive, as if composed of a single mineral. Finally, Hemingway (Fig. 1d), part of a cluster particle from collector L2011, is compositionally similar to Mg-rich olivine and also has a compact appearance suggestive of a single phase. While we have no direct information about whether the IDPs studied here are hydrous or anhydrous, we note that the secondary electron images of a few of the particles show a smooth appearance suggesting that they may be composed predominantly of layer lattice silicates that were flattened upon pressing the particles into the Au foil (cf. SE picture of Eliot in Fig. 6 below).

3.2 H isotopic compositions – ims 3f measurements

Hydrogen isotopic compositions were measured in 16 IDPs with the ims 3f ion microprobe. Results are shown in Table 2 and Fig. 2. Since many of the IDPs are relatively large after they are pressed into the Au foil, it was generally possible to make several measurements on different parts of the IDPs. Thus, the data give some measure of the heterogeneity of

hydrogen isotopic compositions within a given IDP. Most of the particles analyzed have H isotopic compositions that are enriched in D relative to the range of terrestrial values (Fig. 2). The range of D/H ratios within most IDPs is less than a factor of two, but one IDP, Russell, has more variable D-rich compositions, with δD_{SMOW} values ranging from 385 – 3593 ‰ (Table 2). A measurement of the IDP Eucken shows the most D-depleted H isotopic composition seen to date, with $\delta D_{SMOW} = -512 \pm 39$ (Table 2); another portion of this IDP, however, has a normal H isotopic composition.

3.3 C and N isotopic compositions

Carbon and nitrogen isotopic compositions were measured in 39 IDPs. In ten IDPs, however, C and N abundances were too low to acquire statistically significant results in high resolution imaging mode, and no data are reported; these particles are noted in Table 1. Most of these are IDPs whose H isotopic compositions had previously been measured in the 3f ion microprobe and which had very little material remaining for NanoSIMS analysis; however they also include three particles that appear to have inherently low C and N concentrations (Hauptmann, Rolland and von Heidenstam; Table 1). Since N is measured as CN^-, it should be noted that N isotopes can only be measured in the presence of C. Table 3 lists the C and N isotopic compositions of the 29 IDPs for which we were able to obtain data; the average $^{12}C/^{13}C$ and $^{14}N/^{15}N$ ratios are reported for each whole IDP (bulk); in addition, ratios are also reported for localized sub-regions in each IDP that have anomalous N and/or C isotopic compositions (so-called 'hotspots').

All IDPs have normal bulk C isotopic compositions ($\delta^{13}C$ = -47 – 118‰). Fifteen of the 29 also have normal bulk N isotopic compositions ($\delta^{15}N$ = -34 – 57‰); none of these IDPs contain hotspots with anomalous C isotopic compositions, but four of them (Hamsun, Yeats, Reymont and Pirandello) have one or more hotspots that are enriched in ^{15}N with $\delta^{15}N$ values from 590 to 984 ‰ (Table 3). Figure 3 shows the variation of C and N ratios in sub-regions of Bergson, an IDP with normal bulk C and N isotopic compositions (Fig. 3a) and similar data for Pirandello, which also has normal bulk C and N isotopic compositions, but contains two hotspots that are enriched in ^{15}N (Fig. 3b). Also shown are the isotopic ratio images (expressed in delta notation) for both of these IDPs.

The remaining 14 IDPs all have anomalous bulk N isotopic compositions. Most are enriched in ^{15}N, with $\delta^{15}N$ values ranging from 63 to 505 ‰. All but three of these IDPs also contain one or more hotspots that are enriched in ^{15}N, with $\delta^{15}N$ values ranging from 605 to 1303 ‰, the latter representing the largest ^{15}N enrichment observed to date in IDPs. Most of the hotspots have sizes on the order of 250 – 400 nm^2, but a few are larger, 500 – 700 nm^2 (Table 3).

In two cases the ^{15}N-rich hotspots also have anomalous C isotopic compositions. We recently reported the first occurrence of a C isotopic anomaly in an IDP (Floss et al., 2004); the moderate ^{13}C depletion ($\delta^{13}C$ = -70 ‰) was associated with a large ^{15}N enrichment ($\delta^{15}N$ = 1270‰) in a relatively large (0.6 x 1.8 μm^2) region of Benavente dominated by amorphous carbonaceous material. The bulk N isotopic composition of Benavente is also anomalous, with an average $\delta^{15}N$ of 168‰. We have now found a second C isotopic anomaly in the IDP Hesse. Hesse has a bulk^{15}N-rich composition ($\delta^{15}N$ = 349‰) and contains three ^{15}N-enriched hotspots (Fig. 4a); one of these, a region about 245 x 390 nm^2 in size, is also enriched in ^{13}C ($\delta^{13}C$ = 163‰).

Finally, one IDP has a bulk N isotopic composition that is depleted in ^{15}N (Fig. 4b). Eliot has an average $\delta^{15}N$ of -108‰ and contains no other C or N anomalous hotspots.

3.4 O isotopic compositions

Oxygen isotopic imaging was carried out on 26 IDPs. With one exception (Lewis), all of these IDPs were also measured for C and N isotopic compositions (Table 1), although as noted above, three IDPs did not contain sufficient C and N to obtain significant data. Although the bulk IDPs have solar O isotopic compositions (see EXPERIMENTAL), within seven of the particles we identified a total of ten distinct grains with anomalous O isotopic compositions (Table 4). Figure 5 shows the O isotopic ratio images (expressed as delta values) of the IDP Galsworthy; also shown are the $^{28}Si^+$ and secondary electron images acquired at the same time as the O images. Galsworthy contains three grains, labeled G1, G2 and G3 with O isotopic compositions that differ significantly from solar O isotopic ratios; the $^{16}O/^{17}O$ and $^{16}O/^{18}O$ ratios of these grains are given in Table 4. Grain G1 is enriched in ^{18}O, with a slight enrichment in ^{17}O over solar values. Grains G2 and G3 are both strongly enriched in ^{17}O, with moderate depletions in ^{18}O. Eliot, whose O isotopic compositions are shown in Fig. 6, contains the largest grain with anomalous oxygen observed in our IDPs. The grain measures 550 x 700 nm^2 (Table 4) and is

enriched in ^{18}O relative to solar. Most of the presolar grains found in this study are smaller, however, generally on the order of 300 nm in diameter (Table 4). Figure 7 shows the O isotopic compositions of all the presolar grains compared with isotopically normal sub-regions of the IDPs in which they were found. Seven of the grains, including G2 and G3 mentioned above, have elevated $^{17}O/^{16}O$ ratios and solar to moderately depleted $^{18}O/^{16}O$ ratios, whereas the remaining three grains, including E1 and G1 mentioned above, exhibit ^{18}O-enrichments.

3.5 S isotopic compositions

Sulfur isotopic compositions were measured in a subset of 13 IDPs (Table 1). Most of the IDPs selected for S isotopic analysis have anomalous bulk N isotopic compositions, but also included were two IDPs with normal bulk N isotopic compositions and one S-rich particle (Lewis) whose C and N isotopic compositions were not measured. All of the particles analyzed have normal S isotopic compositions. Previous studies of S isotopes in IDPs (e.g., Mukhopadhyay et al., 2003; Stadermann and Bradley, 2003) also show no anomalous S isotopic compositions. Figure 8 shows the S abundances and isotopic variations of two IDPs, one of them a normal c-type IDP, du Gard (Fig. 8a) and the other a S-rich IDP, O'Neill (Fig. 8b). Sulfur isotopic ratios vary by about ± 25 ‰ for $\delta^{34}S$ and ± 50 ‰ for $\delta^{33}S$ within these particles, but there are no statistically significant hotspots with anomalous S isotopic compositions in these or any of the other IDPs measured.

3.6 B and H isotopic compositions

Hydrogen and boron isotopic compositions were measured with the NanoSIMS in 17 IDPs (Table 1). Boron abundances were generally quite low in the IDPs, leading to relatively large statistical variations. However, within the errors (~10%), B isotopic compositions are normal in all of the IDPs measured.

As expected based on the ims 3f results, H isotopic compositions show considerable variability. Six of the 17 IDPs measured have normal H isotopic compositions (Table 5), but the remaining particles exhibit D anomalies of varying magnitude. Some of the IDPs, such as Bunin (Fig. 9a), contain localized hotspots that are strongly enriched in D as well as regions up to several microns in size that are enriched in D, by several hundreds of permil. Other IDPs, such as Reymont (Fig. 9b), contain only D-enriched hotspots in an otherwise isotopically

homogeneous matrix; generally the isotopic composition of the matrix in these IDPs falls within the terrestrial range (-200 to 50 ‰; Hoefs, 1980), but one IDP, Hesse, has an average composition that is slightly D-enriched (Table 5). The hotspots have δD values that range from about 550 to 5000 ‰ and apparent sizes that range from 350 to 700 nm; their true sizes, taking into account the size of the primary beam, are significantly smaller, from about 100 to 500 nm. In some instances D-depleted 'coldspots' also appear to be present in these IDPs, but because of the large errors associated with the low D abundances, we cannot be certain that these are statistically significant.

4. DISCUSSION

4.1 D/H ratios in IDPs

4.1.1 ims 3f measurements

Anomalous H isotopic compositions were first reported in IDPs more than twenty years ago (Zinner et al., 1983), clearly indicating the primitive nature of at least some stratospheric dust. Since that time, D anomalies have been discovered in numerous IDPs, with D/H ratios ranging up to an inferred value of 8 x 10^{-3} (δD_{SMOW} = 50,000‰) for a hotspot in a cluster IDP nicknamed Dragonfly (Messenger et al., 1996; Messenger and Walker, 1998). Such high D/H ratios approach those observed in simple molecules in cold molecular clouds (Millar et al., 1989), suggesting the intact survival of interstellar molecules in some IDPs (Messenger, 2000). Messenger (2000) also noted that both the abundance and magnitude of D anomalies are higher in fragile cluster IDPs than they are in individual IDPs, and suggested that cluster IDPs represent the most primitive solar system material available for laboratory study. For the most part, the cluster IDPs and individual IDPs studied here show similar ranges of D/H ratios, with values that fall within the ranges previously observed in IDPs (Messenger et al., 2003a). However, the two IDPs with the lowest and highest D/H ratios, Eucken and Russell respectively, are both fragments of cluster IDPs; both of these also show the greatest degree of heterogeneity within a single particle (Fig. 2), consistent with the observations of Messenger (2000).

Much of the literature on H isotopic anomalies in IDPs emphasizes the abundant D enrichments commonly observed, but depletions in D have also been found, although they

appear to be less widespread. This may simply be due to the fact that it is more difficult to obtain statistically significant data on depletions in a low abundance isotope. The most D-depleted IDP measured to date is Eucken, with $\delta D_{SMOW} = -512 \pm 39$ ‰ (Table 2). The D/H ratio of 7.6×10^{-5} measured in this particle is 2 to 4 times higher than estimates of the protosolar D/H ratio ($2 - 5 \times 10^{-5}$; Geiss and Gloeckler, 1998) and is similar to an estimate of the D/H ratio of solar system water (8.8×10^{-5}; Robert et al., 2000). However, it seems unlikely that Eucken's D/H ratio is due to the presence of solar system water in the IDP. Although, as mentioned earlier, we have no direct information about the mineralogy of our IDPs, we note that Eucken is a c-type IDP with the typical aggregate structure of anhydrous IDPs. More importantly, a second area of Eucken measured has a 'normal' D/H ratio within the terrestrial range (Table 2, Fig. 2), indicating that the IDP is heterogeneous with respect to its H isotopic composition. It is, thus, more likely that the D depletion is concentrated in a so-called 'coldspot', similar to the D-enriched hotspots often seen in IDPs (e.g., Messenger et al., 1996; Aléon et al., 2001). Unfortunately, we have only limited spatial information about the distribution of H isotopic compositions in this IDP, since it was not possible to carry out NanoSIMS H imaging on this particle.

Deuterium anomalies in IDPs are commonly attributed to an interstellar origin, since there is no nuclear source for D and it is destroyed by conversion into ^{3}He in the early sun. Theoretical treatments of hydrogen fractionation in the interstellar medium typically focus on mechanisms for deuterium enhancement (Geiss and Reeves, 1981; Millar et al., 1989; Sandford et al., 2001), although enhancements of D in one phase (simple molecular species, ices, grain mantles) will necessarily result in depletions in another (e.g., H_2 gas). However, although Eucken is depleted in D relative to terrestrial values, as we noted above, it is still D-enhanced relative to estimates of the protosolar D/H ratio. Thus, it is likely that the 'D coldspot' in Eucken originated by mechanisms similar to those traditionally invoked for the more ubiquitous D enhancements seen in IDPs. Sandford et al. (2001) discussed four mechanisms for D enrichment in organic material: low-temperature gas phase ion-molecule reactions, low-temperature gas-grain reactions, gas phase unimolecular photodissociation, and ultraviolet photolysis in D-enriched ice mantles, each of which is expected to impart distinct signatures. Although it is likely that the material comprising the 'D coldspot' in Eucken is organic, since many D anomalies have been associated with carbonaceous material (Aléon et al., 2001; Keller et al.,

2004; but see also Mukhopadhyay and Nittler, 2003), we unfortunately have no independent information about the carrier of this D depletion. Moreover, an attempt to measure the C and N isotopic compositions of Eucken was unsuccessful, due to the small amount of material remaining after ims 3f analysis.

4.1.2 NanoSIMS measurements

The results from the NanoSIMS H imaging measurements are broadly consistent with those obtained here from the ims 3f ion probe and from earlier studies (e.g., Messenger et al., 2003). Bulk δD values range up to several hundred permil and D hotspot compositions are generally on the order of several thousand permil D enrichment (Table 5). Thus, the H isotopic compositions of the IDP fragments measured with the ims 3f likely represent mixtures of the D hotspots, moderately D-enriched regions and isotopically normal areas observed in the H isotopic imaging measurements. One somewhat surprising observation, given the large number of IDPs measured, is the rather limited magnitude of the D anomalies in the imaging measurements. Although most of the hotspots have δD values higher than 1000 ‰, we did not find any D enrichments approaching the extreme values found in several IDPs by Messenger (2000). One possibility is that there may be a contribution of isotopically normal H from the residual gas in the NanoSIMS sample chamber that dilutes all the observed H anomalies; due to the very low sputtering rate of the NanoSIMS this effect would be more significant than in other ion microprobes such as the 3f. Alternatively, we note that IDPs with extremely large D enrichments are, in fact, rare (Messenger, 2000) and the lack of such enhancements in our IDPs could be real.

For several of the IDPs containing D-rich hotspots, we used the NanoSIMS to make elemental maps of C, N, Al, Si and S, subsequent to the H imaging measurements, in order to see if the hotspots were associated with any of these elements. We found that five hotspots are clearly associated with C and N (Fig. 10), suggesting that the D enrichments are carried by organic material, consistent with other studies (Aléon et al., 2001; Keller et al., 2004). For two other hotspots there are no clear associations with any of the elements that we measured and, in fact, the H imaging measurements for these IDPs suggested that the hotspots were sputtering away by the end of the isotopic analyses. In the larger D-enriched regions, there are no obvious

spatial correlations of any of these elements with the anomalous areas. Usually a mixture of all of the elements are present in these areas.

Previous studies have estimated D hotspot sizes on the order of 1 μm, comparable to the spatial resolution of older SIMS instruments (Aléon et al., 2001; Mukhopadhyay et al., 2002). Our high resolution NanoSIMS studies, however, clearly indicate that D hotspots are significantly smaller, less than 500 nm in diameter. This size range is similar to those of other presolar phases found in IDPs, including ^{15}N-rich hotspots (Table 3), which are probably of interstellar origin, and circumstellar silicates (Table 4), SiC and corundum (Stadermann and Floss, 2004). Recent compound-specific isotopic measurements of organic matter in carbonaceous meteorites show that amino acids, alkanes, alkylbenzenes and alkylnaphthalenes have variable D/H ratios, with D enrichments ranging from ~300 to ~4400 ‰ (Pizzarello and Huang, 2005; Wang et al., 2005), similar to the D isotopic compositions of our hotspots. These organic molecules are probably produced through diverse synthetic pathways in the interstellar medium and may be related to the carriers of the D anomalies in the IDPs.

4.2 Nitrogen and carbon isotopic compositions in IDPs

Nitrogen isotopic anomalies in the form of enrichments in ^{15}N were first reported in IDPs by Stadermann et al. (1989) and have since been found to be as common as H isotopic anomalies (e.g., Messenger et al., 2003a), although the magnitudes of the anomalies are significantly smaller. The results presented here are generally consistent with previous measurements, but extend the range of observed ^{15}N enrichments from ~800 ‰ (Stadermann, 2001) to 1300 ‰ (Table 3), measured in a hotspot in the IDP Kipling. Messenger (2000) noted that cluster IDPs are generally more ^{15}N-rich than individual IDPs and Messenger et al. (2003a) argued that N isotopic anomalies are somewhat more common among cluster IDPs than non-cluster IDPs, although in both cases, the distinctions are not as large as those observed for H isotopic compositions. In this study, six of the eleven cluster IDPs (55 %) and four of the seven individual IDPs (57%) in which we measured the N isotopic compositions have some form of N isotopic anomaly (either ^{15}N-rich hotspots or bulk anomalous compositions), indicating that there is no statistical difference in the abundance of N isotopic anomalies between the cluster and non-cluster IDPs in our study. Although the sheer number of ^{15}N-rich hotspots is greater for the cluster IDPs (Table 3), this is simply due to the fact that many more fragments of cluster IDPs

were analyzed (by definition, only one fragment exists per non-cluster IDP). Normalized to the number of fragments, the proportion of hotspots is virtually identical in cluster and non-cluster IDPs (1.3 vs. 1.5, respectively). Moreover, the most ^{15}N-rich compositions observed among the measured particles are found in the non-cluster IDP Kipling, which has a bulk N isotopic composition of $\delta^{15}N = 505$ ‰ and a hotspot with $\delta^{15}N = 1303$ ‰, (Table 3).

4.2.1 Nitrogen isotopic distributions and carriers in IDPs

The isotopic compositions of both H and N can be quite variable within different portions of the same IDP (Stadermann, 1991; Messenger, 2000) and these variable enrichments of D and ^{15}N have been attributed to the presence of localized concentrations of these isotopes (so-called hotspots). Indeed, the existence of D hotspots is well-documented in IDPs (e.g., McKeegan et al., 1987; Messenger, 2000; this study) as well as in the primitive CR chondrite Renazzo (Guan et al., 1997). One of the earliest NanoSIMS imaging studies showed the presence of a discrete 400 nm sub-grain with a ^{15}N enrichment of ~800 ‰ (Stadermann, 2001), and the results of the present study show that N isotopic anomalies in some cases occur as discrete hotspots with large enrichments in ^{15}N. However, isotopically anomalous N is also present in larger regions that are variably enriched in ^{15}N (albeit to lesser extents than the hotspots), leading to anomalous bulk N compositions for selected IDPs. Thus, the variable enrichments of ^{15}N noted in different fragments of IDPs from past studies, which are essentially bulk or large area measurements (e.g., Stadermann, 1991; Messenger, 2000), can be explained not only by the presence of discrete hotspots in an isotopically normal matrix, but also by the occurrence of larger regions within IDPs that have isotopically anomalous compositions. Recent work has also shown that N isotopic distributions in the CR chondrite Renazzo are similar to those in IDPs (Floss and Stadermann, 2005b); ^{15}N enrichments there also occur as both discrete hotspots and as larger more diffuse regions within the matrix material. This is similar to the situation for H, in which we have observed D-rich hotspots, but also larger regions that are enriched in D (see above). For both isotopic systems, different carriers may account for the two types of anomalies or they could be due to secondary processing, with mixing and dilution of anomalous material resulting in regions with different isotopic compositions.

The ^{15}N enrichments found in IDPs generally appear to be hosted in carbonaceous matter (Stadermann et al., 1989; Aléon et al., 2003; Keller et al., 2004). Keller et al. (2004) found that

IDPs with elevated $^{15}N/^{14}N$ ratios contain N in the form of amine (-NH_2) functional groups, probably attached to other molecules, such as aromatic hydrocarbons. However, the N isotopic analyses of these IDPs are 'bulk' measurements made on relatively large (2-3 μm) fragments and do not provide any information about the internal distribution of the anomalies. Aléon et al. (2003) carried out N isotopic imaging of two IDPs known to contain D-rich organic components and found, based largely on the calibration of CN^-/C^- ratios in different types of organic matter with variable N concentrations, that ^{15}N excesses were associated with strongly N-rich (> 10 wt. %) macromolecular organic components of variable aromaticity and aliphaticity. They also noted that N distributions in these two IDPs reflected mixing between two or more distinct components.

Although we have not made a detailed characterization of possible components of the sort carried out by Aléon et al. (2003), we can make some generalizations about the nature of the isotopically anomalous material present in our IDPs. Figure 11 shows CN^-/C^- ratios plotted against the N isotopic compositions of the bulk IDPs and the anomalous hotspots within them. IDPs with normal bulk N isotopic compositions have CN^-/C^- ratios ranging from 0.8 – 5.4, whereas IDPs with anomalous bulk N isotopic compositions have a more restricted range of CN^-/C^- ratios from 0.7 – 2.1 (Fig. 11a). In addition, the most anomalous IDPs tend to have the lowest CN^-/C^- ratios. These characteristics, together with high C^- signals, suggest that IDPs with anomalous N isotopic compositions are dominated by relatively N-poor carbonaceous matter.

Aléon et al. (2003) determined the CN^-/C^- ratios of a variety of carbonaceous materials with different N abundances and found a linear correlation between the ratios and N concentrations, indicating that CN^- emission is proportional to the product of the C and N concentrations in the sample. The CN^-/C^- ratios of the 1-hydroxybenzotriazole (which has a N concentration of 27.5 wt.%) used as a standard for the C and N measurements in this study range from 1.9 – 4.3, bracketing the values of 2.7 and 3.3 measured by Zinner et al. (1989) and Stadermann (1991) in the Washington University Cameca ims 3f ion microprobe, and is in agreement (within a factor of two) with the calibration scale of Aléon et al. (2003). If the N anomalous material in our IDPs is carbonaceous (a reasonable assumption for the ^{15}N-rich hotspots in our IDPs, which all have high C^- signals), then we can use the calibration scale of Aléon et al. (2003) to estimate the N concentrations of these hotspots. Such estimates will have

a relatively large uncertainty, but can provide some constraints on the type of material carrying these anomalies.

Many of the ^{15}N-rich hotspots found in our IDPs have CN^-/C^- ratios between 0.8 – 1.5 (Fig. 11b), corresponding to N concentrations between 1 – 6 wt.%, which is at the upper end of the range of N concentrations of insoluble organic matter in carbonaceous chondrites (Aléon et al., 2003). A wide variety of CHON grains (composed predominantly of the elements C, H, O, and N) detected in dust from the comet Halley (Jessberger et al., 1988) have N concentrations in this range, and it has been suggested that these may represent organic compounds such as alcohols, ketones, aldehydes, amines and amino acids, with the presence of N indicating amine or nitrile functionalities (Fomenkova et al., 1994). Several hotspots have higher CN^-/C^- ratios of 2 – 3.5, suggesting N concentrations of 10 – 30 wt.%. CHON grains with N concentrations higher than 10 wt.% are rare, but have been observed and could represent acetonitrile polymers or HCN (Fomenkova et al., 1994). Finally, one hotspot from the IDP Hamsun, with a δ^{15}N of 864 ‰, has a very high CN^-/C^- ratio of 9.3, suggesting an unusually high N concentration, in excess of 30 wt.%.

Much of the discussion above is highly speculative and we do not presume to argue that our hotspots consist of the organic compounds mentioned above, as such identifications clearly cannot be made on the basis of CN^-/C^- ratios alone. However, based on the wide range of CN^-/C^- ratios observed in our hotspots, it appears likely that the ^{15}N enrichments are carried by a variety of organic compounds, whose identity will need to be confirmed individually in future work. One promising new technique may be Auger spectroscopy, which can provide compositional information (all elements except H and He can be measured) on a spatial scale comparable to that of the NanoSIMS, without requiring difficult sample preparation (Stadermann et al., 2005b). We carried out exploratory Auger elemental imaging of two ^{15}N-rich hotspots in the IDPs Deledda and Yeats, using the scanning Auger microprobe at PNNL. The hotspot in Deledda seems to consist of N-rich carbonaceous matter, whereas the one from Yeats appears to be dominated by Mg and Si; however, due to instrumental problems, it was not possible to acquire a N map for that hotspot. Quantification of elemental concentrations in the anomalous areas through spot analyses and comparison with standards would be required to provide the additional constraints necessary for identification of the phases present in these hotspots.

Aléon et al. (2003) suggested that submicron-sized hotspots with large ^{15}N excesses, such as those discussed here, might be related to known ^{15}N-rich presolar grains known from meteorites, such as Si_3N_4, SiC or graphite (e.g., Zinner, 2004). We can easily rule out Si_3N_4 or SiC as the source of the ^{15}N enrichments in the IDPs studied here, since there is virtually no Si^- signal from any of the hotspots. The situation is a little more complex for graphite, since the hotspots do seem to consist of carbonaceous material, many with relatively low CN^-/C^- ratios. Graphite grains show a wide range of C isotopic compositions with more limited variations in N isotopic ratios (Hoppe et al., 1995). The fact that our ^{15}N-rich hotspots for the most part are not associated with C isotopic anomalies argues against circumstellar graphite as the carrier phase. Moreover, most graphite grains have significantly lower CN^-/C^- ratios than our ^{15}N-anomalous hotspots. However, some spherulitic aggregate graphites with normal C isotopic ratios and modest ^{15}N enrichments (up to ~500 ‰; Zinner et al., 1995) have CN^-/C^- ratios from about 0.1 – 1, which overlaps the low end of the range of ratios observed in our hotspots, suggesting that this type of graphite could, in principle, be a carrier for the ^{15}N enrichments seen in our IDPs.

The most telling argument against graphite as the carrier phase for the N anomalies observed in our IDPs, however, comes from examination of their abundances and size distributions in meteorites. Graphite abundances in primitive meteorites are about 1–2 ppm, about an order of magnitude lower than abundances of SiC (Zinner, 2004). The nominal size distributions for both graphite and SiC are similar (1–20 μm vs. 0.1–20 μm, respectively), but the peaks in the distributions are very different. Whereas the vast majority of SiC grains are < 0.5 μm in size (Zinner, 2004), the mean size of graphite grains is 2–4 μm and submicron-sized grains make up only a small fraction of all graphites (Bernatowicz et al., 1996). Thus, the abundance of graphite grains in the size range corresponding to the sizes of our hotspots (Table 3) is significantly lower than the 1–2 ppm abundance for all graphite grains and, moreover, is far less than the 800 ppm calculated for the abundance of ^{15}N-rich hotspots in our IDPs. While we cannot absolutely rule out that graphite might be the carrier of one or two of the anomalous hotspots, it clearly cannot account for all the ^{15}N-enriched hotspots present in the IDPs.

4.2.2 Carbon isotopic distributions and carriers in IDPs

Because organic compounds appear to be the source for many of the H and N isotopic anomalies seen in IDPs (Aléon et al., 2001, 2003; Keller et al., 1997, 2004), the lack of abundant isotopic anomalies in C, despite numerous measurements (Messenger et al., 2003a) has been surprising and has prompted speculation as to its cause. Some studies noted that gas-phase reactions are expected to produce C isotopic fractionations, but that different processes produce fractionation effects in opposite directions (Tielens, 1998; Langer et al., 1984; Langer and Graedel, 1989), leading to suggestions that any C isotopic anomalies produced are canceled out by the existence of multiple reaction pathways (Tielens, 1998; Sandford et al., 2001). Others have suggested that isotopic fractionation of C is inhibited by the condensation of CO onto grain surfaces and its participation in grain chemistry (Messenger and Walker, 1998; Messenger et al., 2003a). However, Floss et al. (2004) reported the existence of the first C isotopic anomaly in an interplanetary dust particle. The anomaly, in the form of a ^{13}C depletion, is associated with a ^{15}N enrichment in the IDP Benavente (see Table 3). TEM observations and IR spectra of a FIB lift-out section of the anomalous region show that the anomalies are hosted by organic matter consisting predominantly of aliphatic hydrocarbons (cf. Fig. 4 in Floss et al., 2004). This study showed that C isotopic fractionation does, in fact, occur and provided definitive proof that at least some of the carbonaceous matter in IDPs is itself presolar and is not simply a more 'recent' (e.g., solar system) host substrate for presolar D and ^{15}N-enriched material (Floss et al., 2004).

A second C isotopic anomaly was observed in the IDP Hesse, again associated with a ^{15}N-enriched hotspot (Fig. 5). In contrast to the ^{13}C depletion seen in Benavente, however, the hotspot in Hesse is enriched in ^{13}C by 163 ‰ (Table 3). Preliminary examination of a FIB section extracted from this anomalous region showed that the hotspot was very rich in C. Unfortunately, the section was lost before further measurements could be made to determine the exact nature of the carrier phase. The CN^-/C^- ratio of this anomalous region is, at 0.73, one of the lowest ratios observed in our N-anomalous hotspots and falls within the range of CN^-/C^- ratios observed in spherulitic aggregate graphites (Zinner et al., 1995). We cannot, therefore, rule out the possibility that graphite is the host phase for the C and N isotopic anomalies in this hotspot. However, we noted above that graphite is unlikely to be the carrier of the abundant N hotspots seen in our IDPs. Moreover, studies have shown that, in contrast to carbonaceous

chondrites, graphitic carbon is conspicuously absent from chondritic IDPs (Bradley, 2004; Keller et al., 2000).

4.2.3 Origin of N and C isotopic anomalies in IDPs

Traditionally one of the difficulties associated with understanding the origin of N isotopic anomalies in IDPs has been that, although they are generally thought to be due to chemical fractionation in the interstellar medium (Messenger and Walker, 1998), anomalous N can also be produced nucleosynthetically (e.g., Clayton, 2003). However, a nucleosynthetic origin would suggest that the N isotopic anomalies should be accompanied by isotopically anomalous C, which is not the case for most of the N-anomalous material in our IDPs. A spallation origin is also unlikely, given the magnitudes of the anomalies observed (Geiss and Bochsler, 1982). Despite the common assumption that the ^{15}N enrichments observed in IDPs are due to low temperature interstellar chemical fractionation, there have been few theoretical investigations to provide support for such an origin. An early study by Adams and Smith (1981) suggested that proton exchange with N_2H under typical interstellar cloud conditions could result in a factor of 2 (1000 ‰) enhancement in ^{15}N. A more recent study of ion-molecule exchange reactions involving the most abundant N-bearing species in interstellar clouds indicated a maximum enhancement in ^{15}N of 250 ‰ (Terzieva and Herbst, 2000), whereas another model investigating NH_3 formation in dense molecular clouds suggested a maximum enrichment of 800 ‰ (Charnley and Rodgers, 2002). These models are all consistent with the relatively modest bulk enrichments of ^{15}N observed in our IDPs, but fall short of the values needed to account for the most anomalous compositions found in several of the hotspots (e.g., $\delta^{15}N$ = 1270 – 1303 ‰; Table 3).

Several studies have shown that the solar N isotopic composition is about 30% lighter than the terrestrial one. Hashizume et al. (2000) reported the presence of isotopically light N associated with solar wind implanted hydrogen in lunar regolith grains; these authors estimated that the solar wind N isotopic ratio was depleted in ^{15}N by at least 24 % relative to the terrestrial ratio. Galileo measurements of the Jovian atmosphere indicate a solar N isotopic ratio of $^{15}N/^{14}N = 2.3 \pm 0.3 \times 10^{-3}$ (Owen et al., 2001), which is ~35 % lower than the terrestrial ratio of 3.7×10^{-3}. Since the N isotopic compositions of our IDPs are reported relative to the terrestrial value, the enrichments in ^{15}N indicated in Table 3 may be significantly higher, in many cases higher than can be explained by the theoretical isotopic fractionation models if the anomalies originated

from a gas with a solar N isotopic composition. However, Owen et al. (2001) argued that the $^{15}N/^{14}N$ ratio in a galaxy's interstellar medium should decrease with time, due to the early primary production of ^{15}N and later, secondary addition of ^{14}N, suggesting that the N isotopic composition of the molecular cloud that collapsed to form the solar system should have been more ^{15}N-rich than the local interstellar medium today.

The presence of correlated C and N isotopic anomalies in two of our IDPs requires processes that can produce both effects in the same material. Theoretical studies of interstellar C chemistry show that isotopic fractionations should occur for this element. For example, gas phase ion-molecule reactions can enhance the $^{12}C/^{13}C$ ratios of organic matter (Langer et al., 1984; Langer and Graedel, 1989) to the levels observed in the ^{13}C-depleted region from Benavente (Table 3; Floss et al., 2004), whereas enrichments of ^{13}C, like the one seen in the hotspot from Hesse (Table 3), can be produced through isotope-selective dissociation of CO in dense cloud regions (Tielens, 1998). The work of Charnley and Rodgers (2001) shows that enhanced $^{15}N/^{14}N$ ratios can be produced in NH_3 at high gas phase densities. However, it is not clear whether ^{15}N-rich ammonia can pass on its anomalous N to the organic hosts thought to be responsible for the N (and C) isotopic anomalies in IDPs.

Hashizume et al. (2004) reported isotopic measurements of solar-wind implanted C in lunar regolith grains and suggested that solar C isotopic compositions are depleted in ^{13}C by 10% relative to terrestrial. Combined with observations that solar N is also isotopically light (see above), these results suggest that C and N isotopic compositions are roughly correlated in the solar system, starting from isotopically light solar values towards enrichments in the heavy isotopes among various solar system objects (cf. Fig. 3 of Hashizume et al., 2004). Hashizume et al. (2004) suggest that the elevated ^{13}C of planetary organic carbon, relative to the solar value, could be produced by photodissociation of CO in a warm dense gas, possibly corresponding to the nebula surrounding the proto-sun, which would trigger the formation of organics. Such a process would also need to be compatible with production of the elevated $^{15}N/^{14}N$ ratios seen in planetary organic matter. Clayton (2002) suggested that N isotopic fractionation could occur by photochemical self-shielding and trapping of the photodissociated atoms in refractory minerals such as nitrides. However, it is again not clear that the isotopic compositions thus produced could be transferred from these refractory phases to the organic matter hosting the anomalies in meteorites and IDPs.

The solar depletion in ^{13}C of 10%, relative to terrestrial, postulated by Hashizume et al. (2004) is similar to the magnitude of the ^{13}C depletion observed in the C- and N-anomalous region of Benavente (Table 3; Floss et al., 2004). However, the C isotopic anomaly in Benavente is accompanied by a strong enrichment in ^{15}N and, therefore, cannot simply represent material formed from a reservoir with solar C and N isotopic compositions, as such matter would be expected to be depleted rather than enriched in ^{15}N. The C- and N- anomalous hotspot from Hesse is enriched in the heavy isotopes of both C and N, relative to the solar (and terrestrial) values and could, therefore, in principle have a solar system origin of the type postulated by Hashizume et al. (2004). However, as noted above, there are considerable uncertainties in such a model and it remains to be seen if a nebular origin can adequately account for the C and N isotopic compositions seen in meteoritic organic matter, much less the more extreme compositions observed in IDPs. If future investigations of nebular and interstellar chemistry cannot account for the C and N isotopic fractionations observed in IDPs, circumstellar origins may need to be considered.

4.2.4 Isotopically primitive IDPs

The N isotopic distributions of the IDPs studied here indicate the presence of an isotopically distinct sub-group of IDPs. Of the 29 IDP fragments whose C and N isotopic compositions were measured, 14 have isotopically anomalous bulk N and contain abundant hotspots enriched in ^{15}N (up to 1300 ‰); two of these hotspots also have anomalous C isotopic compositions. Moreover, all 10 of the presolar silicate grains found in this study (see below) occur in IDPs with anomalous bulk N. In contrast, the remaining 15 IDPs have normal bulk N isotopic compositions and, although four of them contain ^{15}N-enriched hotspots, none exhibit C isotopic anomalies and none contain any presolar silicate or oxide grains. We have characterized those IDPs with anomalous bulk N isotopic compositions as isotopically primitive and suggest that bulk N isotopic compositions in IDPs can be used to identify potentially interesting IDPs for further studies, such as the identification of circumstellar silicate or oxide grains or the search for C isotopic anomalies. This is important as it allows the identification of such IDPs without requiring the high spatial resolution of the NanoSIMS for this first step. As discussed in more general terms above, there is statistically no difference between cluster and individual IDPs in terms of their N isotopic compositions: five cluster and three individual particles belong to the

isotopically primitive subgroup of IDPs (which are highlighted in bold in Table 3), whereas six cluster and four individual particles make up the remaining 'normal' IDPs.

Recent N isotopic measurements of the CN spectra of comets Hale-Bopp and C2000 WM1 (LINEAR) give low $^{14}N/^{15}N$ ratios of 140 ± 35 and 140 ± 30, respectively (Arpigny et al., 2003). These values are similar to those observed in many of the ^{15}N-rich hotspots in our IDPs, suggesting a cometary origin for such material. Variations in the ^{15}N enrichments, both in the hotspots and in the bulk N isotopic compositions, probably reflect mixing of different phases (e.g., Arpigny et al., 2003), as well as variable degrees of secondary processing. In this regard, we note that the distributions and ranges of N isotopic compositions in matrix material from the CR chondrite Renazzo are roughly comparable to those seen in our IDPs, but tend to be somewhat less anomalous, probably due to the aqueous alteration experienced by this meteorite (Floss and Stadermann, 2005b).

One of the cluster IDPs that is classified as isotopically primitive is unusual in terms of its N isotopic compositions. We analyzed two fragments of cluster L2036-c24, the IDPs nicknamed Eliot and Pirandello. Whereas Pirandello has a normal bulk N isotopic composition, but contains two hotspots with modest enrichments in ^{15}N, Eliot is unique in being the only IDP in our study that shows a bulk depletion in ^{15}N ($\delta^{15}N$ = -108 ± 9 ‰; Table 3); the anomalous N is not concentrated in a small region of the IDP, but rather is spread out through the bulk of the particle, just as the bulk ^{15}N enrichments are in other isotopically primitive IDPs (Fig. 4b). Depletions in ^{15}N are rare in IDPs; the only other unambiguous occurrence is in a fragment of the cluster IDP Porky, with $\delta^{15}N$ = -93 ± 4 ‰ (Messenger, 2000). Messenger (2000) suggested that the isotopically light N in Porky probably had a nucleosynthetic origin. However, we feel this is unlikely for our IDP, since the isotopic ratios of all the other elements measured in these two particles are normal, with the single exception of a presolar silicate grain found in Eliot (see below). Moreover, the fact that the anomaly is not located in a small discrete phase, like those normally associated with circumstellar grains, argues against a nucleosynthetic origin as well.

The two fragments of this cluster IDP do not have the aggregate textures typical of most of the IDPs studied here (e.g., Fig. 1a,b). Rather, both have very smooth platy appearances, suggesting that they may be hydrous IDPs, consisting predominantly of layer lattice silicates (see SE image of Eliot in Fig. 6). Hydrous IDPs are generally thought to come from asteroidal bodies and have been associated with CM and CI chondrites (Bradley and Brownlee, 1992; Keller et al.,

1992; Rietmeijer, 1992). Although primitive meteorites can have anomalous N, the isotopic compositions are typically ^{15}N-enriched, with the lightest component depleted in ^{15}N by only -20 to -40 ‰ (Alexander et al., 1998), significantly less than the depletion observed in Eliot. On the other hand, the N isotopic composition of Eliot is consistent with measurements of the N isotopic composition of HCN in the comet Hale-Bopp, which has higher than terrestrial values of ^{14}N/^{15}N = 323 ± 46 (Jewitt et al., 1997) and ^{14}N/^{15}N = 330 ± 98 (Ziurys et al., 1999). HCN is considered to be a primary component of cometary ices formed from the condensation of interstellar gases onto the grains comprising cometary nuclei (Irvine et al, 1996). Eliot may be a preserved remnant of such material.

4.2.5 Correlation of H and N in IDPs

As noted above, H and N isotopes have similar types of distributions in IDPs. In both cases anomalies are present as small hotspots with strong enrichments of either D or ^{15}N, and also as larger diffuse regions that have more modest fractionations. Despite this similarity, and the fact that both H and N anomalies are probably carried by carbonaceous matter, these anomalies are not correlated in our IDPs. We measured nine IDPs that contain both D and ^{15}N hotspots and in no case do they sample the same material. In addition, the larger regions with anomalous D compositions are not preferentially associated with areas that have anomalous N isotopic compositions. This lack of a direct correlation between N and H anomalies is not really surprising and is consistent with what has been observed in previous studies (Stadermann, 2001; Mukhopadhyay et al., 2002; Messenger et al., 2003a). The non-correlated effects may be due to different carrier phases for the H and N anomalies and/or due to the fact that different processes are responsible for the generation of the isotopic anomalies (e.g., Sandford et al., 2001).

What is somewhat more surprising is that although the IDPs defined here as isotopically primitive differ in a number of ways from normal IDPs, this difference does not seem to extend to H isotopic compositions. Anomalous H isotopic compositions are not more common in the isotopically primitive sub-group of IDPs than in the other IDPs and, in fact, the D anomalies are almost evenly split between primitive and normal IDPs. Since both H and N isotopic anomalies in IDPs are usually attributed to the preservation of molecular cloud material in these particles (e.g., Messenger and Walker, 1998), we would expect to see more anomalous H isotopic compositions in those IDPs with other primitive characteristics. It is possible that this is simply

a problem of limited statistics. Alternatively, secondary processing may have affected these isotopic systems differently. For example, different volatilities during atmospheric entry heating could cause anomalies in one of the isotopic systems to be lost more readily than the other.

4.3 Presolar silicates

Because IDPs are widely recognized as being among the most primitive of solar system materials available for study, it is perhaps to be expected that they contain presolar grains of circumstellar origin, similar to those commonly found in meteorites (e.g., Zinner, 2004 and references therein). Such grains have recently been found (Stadermann and Floss, 2004, 2005), but the first circumstellar phases to be identified in IDPs were, in fact, silicates (Messenger et al., 2003b). Spectroscopic data indicate abundant submicrometer amorphous and crystalline silicates in the oxygen-rich dust around young main sequence stars and oxygen-rich asymptotic giant branch (AGB) stars (Waters et al., 1996; Demyk et al., 2000) and the discovery in IDPs represented the culmination of a long search for presolar silicates in solar system materials (Messenger and Bernatowicz, 2000; Alexander et al., 2001). Presolar silicate grains have since been found in several primitive meteorites (Nguyen and Zinner, 2004; Nagashima et al., 2004; Mostefaoui and Hoppe, 2004; Kobayashi et al., 2005) as well as numerous IDPs (Floss and Stadermann, 2004) and, most recently, in Antarctic micrometeorites (Yada et al., 2005).

4.3.1 Composition/mineralogy of presolar silicates

Based on the examination of the Si^- and MgO^- images obtained with the NanoSIMS during the O isotopic measurements, all ten of the grains with anomalous oxygen isotopic compositions found in the IDPs studied here can be identified as silicates rather than oxides, which can have similar O isotopic compositions. Moreover, we were able to obtain EDX spectra of seven of the grains, using 5 keV accelerating voltage to minimize contributions from underlying or surrounding material. The excitation volume at 5 keV is estimated to be on the order of 400 – 500 nm for elements with Z = ~10–15 and decreases with increasing atomic number (Goldstein et al., 1992). This is somewhat larger than the size of most of the presolar silicates we have found (Table 4) and, therefore, we expect that some of the signal in our EDX spectra comes from outside of the grains we are analyzing. However, we estimate that the bulk of the signal (~90%) probably comes from the region of interest for most of the grains. Based on

(Mg+Fe)/Si ratios and comparisons with meteoritic olivine and pyroxene EDX spectra, we identify four of the grains as having compositions consistent with pyroxene, two of which are Mg-rich (G1, G3) and two of which are Fe-rich (G2, H1). The remaining three grains (dG1, E1, H2) have (Mg+Fe)/Si ratios that are lower than those of either olivine or pyroxene. It should be emphasized that these identifications are necessarily preliminary and, moreover, are compositional classifications only and do not provide any structural information (i.e., no crystallinity is inferred). Figure 12 shows high magnification microphotographs of the seven grains taken with a field emission (FE) SEM. Most of the grains do not show any strong features that morphologically distinguish them from surrounding material. However, some grains, such as H1, H2 and E1, appear to have aggregate structures with lighter and darker regions, which suggest they may be GEMS.

The nano-scale mineralogy of IDPs requires TEM confirmation of suspected presolar silicates identified from the NanoSIMS analysis. Ultramicrotomy has traditionally been used to prepare thin sections of IDPs for TEM studies (Bradley and Brownlee, 1986; Bradley 1988). While this technique has been used to extract planar sections from meteoritic materials that have been previously analyzed using an ion probe, the technique does potentially lack the site-specific capability required to harvest an anomalous grain from within an IDP (Messenger and Keller, 2005). In recent years focused ion beam (FIB) techniques also have been utilized to prepare thin sections of meteorite material (Heaney et al., 2001; Lee et al., 2003). More significant to this study is the work of Stroud et al., (2002, 2004), who used the FIB lift-out technique to recover grains containing isotopic anomalous signatures identified within meteoritic material. Using an in situ recovery method (Graham et al., 2004), we were able to successfully extract a section of one of the presolar silicates, the largest grain E1 from Eliot (Fig. 13). A detailed TEM examination of its petrography showed that this presolar grain, as suggested by the FE-SEM photo (Fig. 12), does indeed consist of multiple GEMS regions (Fig. 14). Elemental mapping and EDX analyses of the section indicate that the GEMS are very Mg-rich.

Their small sizes and the presence of abundant silicates of solar system origin make the identification of presolar silicate grains a non-trivial task. In a limited number of cases, presolar silicate grains found in IDPs and primitive meteorites have been classified as olivine, pyroxene and GEMS (Messenger et al., 2003b; Mostefaoui and Hoppe, 2004; Nguyen and Zinner, 2004). Many of these identifications are compositional, based on EDX spectra (e.g., Mostefaoui and

Hoppe, 2004; Nguyen and Zinner, 2004) and are subject to the same uncertainties discussed above for our grains. However, Messenger et al. (2003b) were able to confirm the circumstellar origin of two GEMS and one forsterite grain previously identified by TEM. Moreover, Nguyen et al. (2005) found that a Ca-bearing grain, tentatively identified as clinopyroxene (Nguyen and Zinner, 2004) and extracted from a grain dispersion mount using a FIB lift-out, had an amorphous structure with no rims or sub-grains and a non-stoichiometric composition containing Si, Mg, Fe, Al and Ca. Clearly the identification of presolar silicate grains is still in its infancy. While the FIB lift-out technique is promising, the preparation of such thin sections can result in substantial loss of material. Another promising new technique may be the use of scanning Auger spectroscopy to obtain more precise compositional information of in situ silicate grains after their isotopic identification as stardust with the NanoSIMS, as discussed above for the identification of ^{15}N-rich hotspots.

Using the scanning Auger microprobe at PNNL we were able to locate and make Auger elemental maps of presolar grain D1 from the IDP Deledda. This grain is about 160 nm in diameter and is an Fe-rich silicate (Fig. 15). Fe-Mg silicates, such as olivine and pyroxene, are expected to have Mg-rich compositions under conditions of equilibrium condensation in the stellar winds of oxygen-rich RGB and AGB stars (Ferrarotti and Gail, 2001). Enrichment of Fe in presolar silicates has been observed in primitive meteorites and has been considered to be of secondary origin, due to nebular or parent body processing (Nguyen and Zinner, 2004). However, another possibility is that this may be a primary feature (Floss et al., 2005). Non-equilibrium condensation in stellar outflows is expected to produce silicates with higher Fe contents than equilibrium condensation (Gail, 2003), and amorphous silicates observed around oxygen-rich stars are thought to be Fe-rich in order to explain their higher absorptivity in the near-infrared (Molster et al., 2002). Indeed, TEM analysis of a FIB lift-out section of one presolar silicate from Acfer 094 shows it to be an amorphous silicate containing abundant Fe (Nguyen et al., 2005). Deledda appears to be an anhydrous IDP, which is unlikely to have experienced significant secondary processing. Thus, the presolar grain D1 may represent a primary Fe-rich silicate condensate that formed under non-equilibrium conditions.

4.3.2 Presolar silicates in IDPs and meteorites

We calculated the abundance of presolar grains in our IDPs by dividing the area of the grains by the total area of the IDPs measured, and obtained an abundance of ~120 ppm. If, as we argued above, IDPs with anomalous bulk N isotopic compositions represent a distinct population of isotopically primitive IDPs, we can calculate an abundance of presolar grains in this sub-group of IDPs of ~375 ppm, three times higher than the abundance in all of our IDPs. This value is more than an order of magnitude lower than an initial estimate of ~5500 ppm for presolar silicates in IDPs (Messenger et al., 2003b). However, the population of presolar silicates in the study of Messenger et al. (2003b) was dominated by one relatively large grain (~1μm), whereas most presolar silicates in IDPs are significantly smaller (Table 4), thus skewing the statistics of this early study. A calculation incorporating the data of Messenger et al. (2003b) and the data from this study leads to an average presolar silicate abundance of ~810 ppm in isotopically primitive IDPs.

Presolar silicates have been found in a number of primitive meteorites, including Acfer 094 (ungrouped C3), Adelaide (ungrouped C3) NWA 530 (CR2), Bishunpur (LL3.1), Semarkona (LL3.0), ALHA 77307 (CO3.0) and Y-81025 (CO3.0) (Mostefaoui et al., 2003; Mostefaoui and Hoppe, 2004; Nagashima et al., 2004; Kobayashi et al., 2005; Nguyen et al., 2005), with abundances ranging from 3 ppm in NWA 530 (Nagashima et al., 2004) up to 176 ppm in Acfer 094 (Nguyen et al., 2005). Although the abundance estimates in both meteorites and IDPs are still plagued by low statistics and are rapidly evolving as more grains are found, it appears clear that presolar silicate abundances are significantly higher in IDPs than in most primitive meteorites, emphasizing the primitive nature of interplanetary dust particles relative to other solar system materials. Moreover, except for nanodiamonds (which may not all be presolar), silicates appear to be the most common presolar phase, with abundances that are one to two orders of magnitude greater than presolar SiC, graphite and oxide grains (Zinner, 2004). This is consistent with observations that both amorphous and crystalline silicates (enstatite, forsterite and diopside) are abundant in the dust shells around evolved oxygen-rich stars (Waters et al., 1996; Demyk et al., 2000).

The oxygen isotopic compositions of presolar silicate grains in IDPs and primitive meteorites can be compared with the compositions observed in presolar oxide grains from primitive meteorites. Nittler et al. (1997) divided the presolar oxide grains they found into four

groups that probably indicate different types of stellar sources. Group 1 grains have ^{17}O excesses and solar to moderately depleted ^{18}O. Group 2 grains also have ^{17}O excesses and large ^{18}O depletions. Group 3 grains are enriched in ^{16}O and Group 4 grains have enrichments of ^{17}O and ^{18}O. In primitive meteorites, presolar silicate grains with oxygen isotopic compositions consistent with all four groups have been found (Nguyen et al., 2005; Kobayashi et al., 2005), although Group 1 grains are by far the most common, as they are among the oxide grains as well (Nittler et al., 1997). In IDPs, three of the four groups are represented in the presolar silicate population, with Group 1 grains the most common; no grains with oxygen isotopic compositions consistent with Group 2 oxide grains have been observed.

Seven of the ten presolar silicate grains from this study have oxygen isotopic compositions consistent with Group 1 oxide grains (Fig. 7). These grains most likely have an origin in red giant (RG) or asymptotic giant branch (AGB) stars. Their isotopic compositions are determined by convective mixing of the remnants of main sequence H core burning in the stellar envelope as the star evolves and leaves the main sequence to become a red giant, a process known as the first dredge-up (Nittler, 1998). Following this phase and core He-burning, the star enters the AGB phase. Variations in stellar masses, which determine the depth of the convective envelope, and in the initial compositions of the parent stars account for the different $^{17}O/^{16}O$ ratios observed in the grains.

The remaining three presolar silicate grains exhibit the enrichments in ^{18}O and ^{17}O found in Group 4 oxide grains (Fig. 7). The origin of such grains is more problematic and several possibilities have been proposed. Nittler et al. (1997) suggested that low mass, high metallicity stars could produce grains with the appropriate oxygen isotopic compositions, but noted that it is unlikely that such stars, which would be very old, would have been present to contribute dust to our presolar cloud. Origins in the ejecta of a type II supernova were suggested for a presolar corundum grain from Semarkona (Choi et al., 1998) and for a presolar silicate grain with a very large ^{18}O-enrichment from an IDP (Messenger and Keller, 2004). However, Mostefaoui and Hoppe (2004) argued for an origin in the wind of a RG or AGB star for an ^{18}O-rich presolar grain from Acfer 094 on the basis of Si and Fe isotopic ratios. In the absence of additional isotopic measurements, a specific stellar source cannot be determined for the Group 4 silicate grains from this study.

4.3.3 The origin of GEMS

GEMS are an abundant component of anhydrous chondritic porous IDPs. These sub-micrometer glassy objects have long been of particular interest because it has been proposed that they may be the irradiated remnants of cosmically abundant interstellar silicate grains, with which they share many spectral features (Bradley, 1994; Bradley et al., 1999). Debate over the origin of GEMS has recently intensified with the observation that although some GEMS grains have oxygen isotopic ratios indicating a presolar origin (Messenger et al., 2003b; this study), most have solar oxygen isotopic compositions (Stadermann and Bradley, 2003). Based on these observations, Keller and Messenger (2004) proposed that most GEMS have an origin in the inner solar system and were transported to the comet-forming regions through bipolar outflows during early accretion of the protoplanetary disk. Bradley and Dai (2004) have argued, conversely, that a non-solar isotopic composition is not a reliable indicator of whether or not GEMS have a presolar origin. Bradley (1994) proposed that GEMS formed by irradiation processing of crystalline mineral grains. During this process crystalline grains become progressively amorphized and chemically homogenized. Bradley and Dai (2004) suggest that isotopic compositions also become homogenized. Moreover, these authors used crystallographic analyses of relict grains embedded in GEMS to show that the GEMS are pseudomorphs of these grains, indicating that they are the remnants of the original crystals from which the GEMS formed. In some instances, compositional data also provided supporting evidence for an origin of GEMS through irradiation of pre-existing crystalline mineral grains (Bradley and Dai, 2004).

One of the presolar grains observed in this study, E1, has been clearly identified as GEMS (Fig. 14) and two others, H1 and H2, are likely candidates, based on their aggregate appearance in FE-SEM photos (Fig. 12). Although the E1 GEMS from Eliot do not seem to contain any relict grains, they have very Mg-rich compositions, as noted above, suggesting that they may have formed from interstellar irradiation of pre-existing circumstellar forsterite.

CONCLUSIONS

NanoSIMS isotopic imaging of a suite of IDPs shows that N isotopic compositions can be used to characterize IDPs and identify those that share a variety of primitive isotopic compositions, including the presence of abundant presolar silicate grains. H and N isotopic

compositions in these IDPs show similar distributions; fractionations are present both as small D-rich or ^{15}N-rich hotspots and as larger more diffuse anomalous regions. However, H and N anomalies are not correlated and D enrichments are not preferentially associated with isotopically primitive IDPs. This may be due to a difference in the effects of secondary processing on the isotopic systems involved.

Presolar silicate grains in the IDPs show a variety of isotopic compositions that are similar to the oxygen isotopic compositions of presolar silicate and oxide grains from primitive meteorites. Most of the grains have isotopic ratios consistent with origins from red giant or asymptotic giant branch stars. Presolar silicate abundances in the isotopically primitive IDPs are ~375 ppm, significantly higher than in most primitive meteorites, emphasizing the primitive nature of IDPs compared to most other solar system materials.

ACKNOWLEDGEMENTS

We thank Tim Smolar for maintenance of the NanoSIMS. A portion of the research described herein was carried out in the Environmental Molecular Sciences Laboratory, a national scientific user facility sponsored by the Department of Energy's Office of Biological and Environmental Research and located at Pacific Northwest National Laboratory. This work was supported by NASA grant NNG04GG49G to C. F and NAG5-10632 and NAG5-10696 to J. B. This work was in part performed under the auspices of the U.S. Department of Energy, National Nuclear Security Administration by University of California, Lawrence Livermore National Laboratory under contract No. W-7405-Eng-48. Mike Bernas (FEI Company) is thanked for extensive assistance and guidance with the FIB work of selected IDPs.

REFERENCES

Adams N. G. and Smith D. (1981) $^{14}N/^{15}N$ isotope fractionation in the reaction $N_2H^+ + N_2$: interstellar significance. *Astrophys. J.* **247**, L123-L125.

Aléon J., Engrand C., Robert F., and Chaussidon M. (2001) Clues to the origin of interplanetary dust particles from the isotopic study of their hydrogen-bearing phases. *Geochim. Cosmochim. Acta* **65**, 4399-4412.

Aléon J., Robert F., Chaussidon M., and Marty B. (2003) Nitrogen isotopic composition of macromolecular organic matter in interplanetary dust particles. *Geochim. Cosmochim. Acta* **67**, 3773-3787.

Alexander C. M. O'D., Russell S. S., Arden J. W., Ash R. D., Grady M. M., and Pillinger C. T. (1998) The origin of chondritic macromolecular organic matter: a carbon and nitrogen isotope study. *Meteorit. Planet. Sci.* **33**, 603-622.

Alexander C. M. O'D., Nittler L. R., and Tera F. (2001) The search of presolar silicates and the ^{54}Cr carrier. *Lunar Planet. Sci. XXXII*, #2191.

Arpigny C., Jehin E., Manfroid J., Hutsemékers D., Schultz R., Stüwe J. A., Zucconi J.-M., and Ilyin I. (2003) Anomalous nitrogen isotope ratio in comets. *Science* **301**, 1522-1524.

Bernatowicz T., Cowsik R., Gibbons P. C., Lodders K., Fegley B., Amari S., and Lewis R. S. (1996) Constraints on stellar grain formation from presolar graphite in the Murchison meteorite. *Astrophys. J.* **472**, 760-782.

Bradley J. P. (1988) Analysis of chondritic interplanetary dust thin-sections. *Geochim. Cosmochim. Acta* **52**, 889-900.

Bradley J. P. (1994) Chemically anomalous preaccretionally irradiated grains in interplanetary dust from comets. *Science* **265**, 925-929.

Bradley J. P. (2004) Interplanetary dust particles. In *Meteorites, Planets and Comets*, A. M. Davis, Ed. (Vol. 1, Treatise on Geochemistry, H. D. Holland, K. K. Turekian, Exec. Eds.) pp. 689-711. Elsevier Science.

Bradley J. P. and Brownlee D. E. (1986) Cometary particles: thin sectioning and electron beam analysis. *Science* **231**, 1542-1544.

Bradley J. P. and Brownlee D. E. (1992) An interplanetary dust particle linked directly to type CM meteorites and an asteroidal origin. *Science* **251**, 549-552.

Bradley J. P. and Dai Z. R. (2004) Mechanism of formation of glass with embedded metal and sulfides. *Astrophys. J.* **617**, 650-655.

Bradley J. P., Keller L. P., Snow T. P., Hanner M. S., Flynn G. J., Gezo J. C., Clemett S. J., Brownlee D. E., and Bowey J. E. (1999) An infrared spectral match between GEMS and interstellar grains. *Science* **285**, 1716-1718.

Brownlee D. E., Ferry G. V., and Tomandl D. (1976) Stratospheric aluminum oxide. *Science* **191**, 1270-1271.

Brownlee D. E., Joswiak D. J., Schlutter D. J., Pepin R. O., Bradley J. P., and Love S. G. (1995) Identification of individual cometary IDPs by thermally stepped He release. *Lunar Planet. Sci. XXVI*, 183-184.

Charnley S. B. and Rodgers S. D. (2002) The end of interstellar chemistry as the origin of nitrogen in comets and meteorites. *Astrophys. J.* **569**, L133-L137.

Choi B.-G., Huss G., Wasserburg G., and Gallino R. (1998) Presolar corundum and spinel in ordinary chondrites: origins from AGB stars and a supernova. *Science* **282**, 1284-1289.

Clayton D. (2003) *Isotopes in the Cosmos: Hydrogen to Gallium*. Cambridge University Press, 314 pp.

Clayton R. N. (2002) Self-shielding in the solar nebula. *Nature* **415**, 860-861.

Demyk A., Dartois E., Wiesemeyer H., Jones A. P., and d'Hendecourt L. (2000) Structure and chemical composition of the silicate dust around OH/IR stars. *Astron. Astrophys.* **364**, 170-178.

Ferrarotti A. S. and Gail H.-P. (2001) Mineral formation in stellar winds II. Effects of Mg/Si abundance variations on dust composition in AGB stars. *Astron. Astrophys.* **371**, 133-151.

Floss C. and Stadermann F. J. (2002) NanoSIMS measurements of nitrogen isotopic distributions in IDPs and Renazzo: uniform ^{15}N enrichment in a chondritic IDP. *Lunar Planet. Sci. XXXIII*, #1350.

Floss C. and Stadermann F. J. (2003) Complementary carbon, nitrogen and oxygen isotopic imaging of interplanetary dust particles: presolar grains and an indication of a carbon isotopic anomaly. *Lunar Planet. Sci. XXXIV*, #1238.

Floss C. and Stadermann F. J. (2004) Isotopically primitive interplanetary dust particles of cometary origin: evidence from nitrogen isotopic compositions. *Lunar Planet. Sci. XXXV*, #1281.

Floss, C. and F. J. Stadermann (2005a) NanoSIMS D/H imaging of isotopically primitive interplanetary dust particles. *Lunar Planet. Sci. XXXVI*, #1423.

Floss C. and Stadermann F. J. (2005b) Presolar (circumstellar and interstellar) phases in Renazzo: the effects of parent body processing. *Lunar Planet. Sci. XXXVI*, #1390.

Floss C., Stadermann F. J., Bradley J. P., Dai Z. R., Bajt S., and Graham G. (2004) Carbon and nitrogen isotopic anomalies in an anhydrous interplanetary dust particle. *Science* **303**, 1355-1358.

Floss C., Stadermann F. J., Nguyen A., Zinner E., and Lea A. S. (2005) High Fe contents in presolar silicate grains: primary feature or the result of secondary processing? *Meteorit. Planet. Sci.*, submitted.

Fomenkova M. N., Chang S., and Mukhin L. M. (1994) Carbonaceous components in the comet Halley dust. *Geochim. Cosmochim. Acta* **58**, 4503-4512.

Gail H.-P. (2003) Formation and evolution of minerals. In *Astromineralogy* (ed. T. Henning), pp. 55-120. Springer Verlag.

Geiss J. and Reeves H. (1981) Deuterium in the solar system. *Astron. Astrophys.* **93**, 189-199.

Geiss J. and Bochsler P. (1982) Nitrogen isotopes in the solar system. *Geochim. Cosmochim. Acta* **46**, 529-548.

Geiss J. and Gloeckler G. (1998) Abundances of deuterium and helium-3 in the protosolar cloud. *Space Sci. Rev.* **84**, 239-250.

Giannuzzi L. A., Kempshall B. W., Schwarz S. M., Lomness J. K., Prenitzer B. I., and Stevie F. A. (2004) FIB lift-out specimen preparation techniques – ex situ and in situ methods. In *Introduction to Focused Ion Beam – Instrumentation, Theory, Techniques and Practice*. (L. A. Giannuzzi and F. A. Stevie, Eds.), Springer-Verlag, pp. 201-228.

Goldstein J. I., Newbury D. E., Echlin P., Joy D. C., Romig A. D., Lyman C. E., Fiori C., and Lifshin E. (1992) *Scanning Electron Microscopy and X-Ray Microanalysis*. Plenum Press, 820 pp.

Graham G. A., Bradley J. P., Bernas M., Stroud R. M., Dai Z. R., Floss C., Stadermann F. J., Snead C. J., and Westphal A. J. (2004) Focused ion beam recovery and analysis of interplanetary dust particles (IDPs) and Stardust analogues. *Lunar Planet. Sci. XXXV*, #2044.

Guan Y., Messenger S., and Walker R. M. (1997) The spatial distribution of D-enrichments in Renazzo matrix. *Lunar Planet. Sci. XXVIII*, 489-490.

Hashizume K., Chaussidon M., Marty B., and Robert F. (2000) Solar wind record on the Moon: deciphering presolar from planetary nitrogen. *Science* **290**, 1142-1145.

Hashizume K., Chaussidon M., Marty B., and Terada K. (2004) Protosolar carbon isotopic composition: implications for the origin of meteoritic organics. *Astrophys. J.* **600**, 480-484.

Heaney P. J., Vicenzi E. P., Giannuzzi L. A., and Livi K. J. T. (2001) Focused ion beam milling: a method of site-specific sample extraction for microanalysis of Earth and planetary materials. *Am. Mineral.* **86**, 1094-1099.

Hoefs J. (1980) *Stable Isotope Geochemistry*. Springer Verlag, 140 pp.

Hoppe P., Amari S., Zinner E., and Lewis R. S. (1995) Isotopic compositions of C, N, O, Mg, and Si, trace element abundances, and morphologies of single circumstellar graphite grains in four density fractions from the Murchison meteorite. *Geochim. Cosmochim. Acta* **59**, 4029-4056.

Irvine W. M., Bockelee-Morvan D., Lis D. C., Matthews H. E., Biver N., Crovisier J., Davies J. K., Dent W. R. F., Gautier D., Godfrey P. D., Keene J., Lovell A. J., Owen T., Phillips T.

G., Rauer H., Schloerb F. P., Senay M., and Young K. (1996) Spectroscopic evidence for interstellar ices in comet Hyakutake. *Nature* **383**, 418-420.

Jessberger E. K., Christoforidis A., and Kissel J. (1988) Aspects of the major element composition of Halley's dust. *Nature* **332**, 691-695.

Jewitt D. C., Matthews H. E., Owen T., and Meier R. (1997) Measurements of $^{12}C/^{13}C$, $^{14}N/^{15}N$, and $^{32}S/^{34}S$ ratios in comet Hale-Bopp (C/1995 O1). *Science* **278**, 90-93.

Keller L. P. and Messenger S. (2004) On the origin of GEMS. *Lunar Planet. Sci. XXXV*, #1985.

Keller L. P., Thomas K. L., and McKay D. S. (1992) An interplanetary dust particle with links to CI chondrites. *Geochim. Cosmochim. Acta* **56**, 1409-1412.

Keller L. P., Messenger S., Miller M., and Thomas K. L. (1997) Nitrogen speciation in a ^{15}N-enriched interplanetary dust particle. *Lunar Planet. Sci. XXVIII*, 707-708.

Keller L. P., Messenger S., and Bradley J. P. (2000) Analysis of a deuterium-rich interplanetary dust particle (IDP) and implications for presolar material in IDPs. *J. Geophys. Res.* **105**, 10397-10402.

Keller L. P., Messenger S., Flynn G. J., Clemett S. J., Wirick S., and Jacobsen C. (2004) The nature of molecular cloud material in interplanetary dust. *Geochim. Cosmochim. Acta* **68**, 2577-2589.

Kobayashi S., Tonotani A., Sakamoto N., Nagashima K., Krot A. N., and Yurimoto H. (2005) Presolar silicate grains from primitive carbonaceous chondrites Y-81025, ALHA77307, Adelaide and Acfer 094. *Lunar Planet. Sci. XXXVI*, #1931.

Langer W. D. and Graedel T. E. (1989) Ion-molecule chemistry of dense interstellar clouds: nitrogen-, oxygen-, and carbon-bearing molecule abundances and isotopic ratios. *Astrophys. J. Suppl. Series* **69**, 241-269.

Langer W. D., Graedel T. E., Frerking M. A., and Armentrout P. B. (1984) Carbon and oxygen isotope fractionation in dense molecular clouds. *Astrophys. J.* **277**, 581-604.

Lee M. R., Bland P. A., and Graham G. A. (2003) Preparation of TEM samples by focused ion beam (FIB) techniques: applications to the study of clays and phyllosilicates in meteorites. *Mineral. Mag.* **67**, 581-592.

Lodders K. and Fegley B. (1998) *The Planetary Scientist's Companion*. Oxford University Press. 371 pp.

McKeegan K. D. (1987) Ion microprobe measurements of H, C, O, Mg, and Si isotopic abundances in individual interplanetary dust particles. Ph.D. Thesis, Washington University. 187 pp.

McKeegan K. D., Walker R. M., and Zinner E. (1985) Ion microprobe isotopic measurements of individual interplanetary dust particles. *Geochim. Cosmochim. Acta* **49**, 1971-1987.

McKeegan K. D., Swan P., Walker R. M., Wopenka B., and Zinner E. (1987) Hydrogen isotopic variations in interplanetary dust particles. *Lunar Planet. Sci. XVIII*, 627-628.

Messenger S. (2000) Identification of molecular-cloud material in interplanetary dust particles. *Nature* **404**, 968-971.

Messenger S. and Bernatowicz T. (2000) Search for presolar silicates in Acfer 094. *Meteorit. Planet. Sci.* **35**, A109.

Messenger S. and Keller L. P. (2004) A supernova silicate from a cluster IDP. *Meteorit. Planet. Sci.* **39**, A68.

Messenger S. and Keller L. P. (2005) Association of presolar grains with molecular cloud material in IDPs. *Lunar Planet. Sci. XXXVI*, #1846.

Messenger S. and Walker R. M. (1998) Evidence for molecular cloud material in meteorites and interplanetary dust. In *Astrophysical Implications of the Laboratory Study of Presolar Materials* (ed. T. J. Bernatowicz and E. Zinner), American Institute of Physics, pp. 545-564.

Messenger S., Walker R. M., Clemett S. J., and Zare R. N. (1996) Deuterium enrichments in cluster IDPs. *Lunar Planet. Sci. XXVII*, 867-868.

Messenger S., Stadermann F. J., Floss C., Nittler L. R., and Mukhopadhyay S. (2003a) Isotopic signatures of presolar materials in interplanetary dust. *Space Sci. Rev.* **106**, 155-172.

Messenger S., Keller L. P., Stadermann F. J., Walker R. M., and Zinner E. (2003b) Samples of stars beyond the solar system: silicate grains in interplanetary dust. *Science* **300**, 105-108.

Millar T. J., Bennett A., and Herbst E. (1989) Deuterium fractionation in dense interstellar clouds. *Astrophys. J.* **340**, 906-920.

Molster F. J., Waters L. B. F. M., Tielens A. G. G. M., Koike C., and Chihara H. (2002) Crystalline silicate dust around evolved stars III. A correlations study of crystalline silicate features. *Astron. Astrophys.* **382**, 241-255.

Mostefaoui S. and Hoppe P. (2004) Discovery of abundant in situ silicate and spinel grains from red giant stars in a primitive meteorite. *Astrophys. J.* **613**, L149-L152.

Mostefaoui S., Hoppe P., Marhas K. K., and Groener E. (2003) Search for in situ presolar oxygen-rich dust in meteorites. *Meteorit. Planet. Sci.* **38**, A99.

Mukhopadhyay S. and Nittler L. R. (2003) D-rich water in interplanetary dust particles. *Lunar Planet. Sci. XXXIV*, #1941.

Mukhopadhyay S., Nittler L. R., and Messenger S. (2002) Hydrogen, carbon, and nitrogen isotopic imaging of cluster IDPs. *Meteorit. Planet. Sci.* **37**, A104.

Mukhopadhyay S., Nittler L. R., Messenger S., Brownlee D. E., Joswiak D. J., and Keller L. P. (2003) Sulfur isotopic compositions of interplanetary dust particles. *Meteorit. Planet. Sci.* **38**, A149.

Nagashima K., Krot A. N., and Yurimoto H. (2004) Stardust silicates from primitive meteorites. *Nature* **428**, 921-924.

Nguyen A. N. and Zinner E. (2004) Discovery of ancient silicate stardust in a meteorite. *Science* **303**, 1496-1499.

Nguyen A. N., Zinner E., and Stroud R. M. (2005) Continued characterization of presolar silicate grains from the Acfer 094 carbonaceous chondrite. *Lunar Planet. Sci. XXXVI*, #2196.

Nittler L. R. (1998) Presolar oxide grains in meteorites. In *Astrophysical Implications of the Laboratory Study of Presolar Materials* (eds. T. J. Bernatowicz and E. Zinner), pp. 59-82. American Institute of Physics.

Nittler L. R., Alexander C. M. O. D., Gao X., Walker R. M., and Zinner E. (1997) Stellar sapphires: the properties and origins of presolar Al_2O_3 in meteorites. *Astrophys. J.* **483**, 475-495.

Owen T., Mahaffy P. R., Nieman H. B., Atreya S., and Wong M. (2001) Protosolar nitrogen. *Astrophys. J.* **553**, L77-L79.

Pizzarello S. and Huang Y. (2005) The deuterium enrichment of individual amino acids in carbonaceous meteorites: a case for the presolar distribution of biomolecule precursors. *Geochim Cosmochim. Acta* **69**, 599-605.

Rietmeijer F. J. M. (1992) Interplanetary dust particle L2005T12 directly linked to type CM chondrite petrogenesis. *Lunar Planet. Sci XXIII*, 1153-1154.

Robert F., Gautier D., and Dubrulle B. (2000) The solar system D/H ratio: observations and theory. *Space Sci. Rev.* **92**, 201-224.

Sandford S. A., Bernstein M. P., and Dworkin J. P. (2001) Assessment of the interstellar processes leading to deuterium enrichment in meteoritic organics. *Meteorit. Planet. Sci.* **36**, 1117-1133.

Stadermann F. J., Walker R. M., and Zinner E. (1989) Ion microprobe measurements of nitrogen and carbon isotopic variations in individual IDPs. *Meteoritics* **24**, 327.

Stadermann F. J. (1991) Messung von Isotopen- und Elementhäufigkeiten in einzelnen Interplanetaren Staubteilchen mittels Sekundärionen-Massenspektrometrie. Ph.D. Dissertation, Ruprecht-Karls-Universität, Heidelberg. 97 pp.

Stadermann F. J. (2001) Hydrogen, carbon, and nitrogen isotopic imaging of sub-micron components from interplanetary dust particles. *Lunar Planet. Sci. XXXII*, #1792.

Stadermann F. J. and Bradley J. P. (2003) The isotopic nature of GEMS in interplanetary dust particles. *Meteorit. Planet. Sci.* **38**, A123.

Stadermann F. J. and Floss C. (2004) Discovery of presolar corundum (and SiC?) in an interplanetary dust particle. *Workshop on Chondrites and the Protoplanetary Disk*, #9045.

Stadermann F. J. and Floss C. (2005) Circumstellar corundum and silicon carbide in interplanetary dust particles. *Geochim. Cosmochim. Acta*, in preparation.

Stadermann F. J., Walker R. M., and Zinner E. (1989) Ion microprobe measurements of nitrogen and carbon isotopic variations in individual IDPs. *Meteoritics* **24**, 327.

Stadermann F. J., Croat T. K., Bernatowicz T., Amari S., Messenger S., Walker R. M., and Zinner E. (2005a) Supernova graphite in the NanoSIMS: carbon, oxygen and titanium isotopic compositions of a spherule and its TiC sub-components. *Geochim. Cosmochim. Acta* **69**, 177-188.

Stadermann F. J., Floss C., Zinner E., Nguyen A., and Lea A. S. (2005b) Auger spectroscopy as a complement to NanoSIMS studies of presolar materials. *Meteorit. Planet. Sci.*, submitted.

Stroud R. M., Nittler L. R., and Alexander C. M. O'D. (2002) Transmission electron microscopy of a presolar corundum grain. *Meteorit. Planet. Sci.* **37**, A137.

Stroud R. M., Nittler L. R., and Alexander C. M. O'D. (2004) Polymorphism in presolar Al_2O_3 grains from asymptotic giant branch stars. *Science* **305**, 1455-1457.

Terzieva R. and Herbst E. (2000) The possibility of nitrogen isotopic fractionation in interstellar clouds. *Mon. Not. R. Astron. Soc.* **317**, 563-568.

Tielens A. G. G. M. (1998) Deuterium and interstellar chemical processes. In *Astrophysical Implications of the Laboratory Study of Presolar Materials* (eds. T. Bernatowicz and E. Zinner), American Institute of Physics, pp. 523-544.

Wang Y., Huang Y., Alexander C. M. O'D., Fogel M., and Cody G. (2005) Molecular and compound-specific hydrogen isotope analyses of insoluble organic matter from different carbonaceous chondrite groups. *Geochim Cosmochim. Acta* **69**, 3711-3721.

Waters L. B. F. M., Molster F. J., de Jong T., Beintema D. A., Waelkens C., Boogert A. C. A., Boxhoorn D. R., de Graauw T., Drapatz S., Feuchtgruber H., Genzel R., Helmich F. P., Heras A. M., Huygen R., Izumiura H., Justtanont K., Kester D. J. M., Kunze D., Lahuis F., Lamers H. J. G. L. M., Leech K. J., Loup C., Lutz D., Morris P. W., Price S. D., Roelfsema P. R., Salama A., Schaeidt S. G., Tielens A. G. G. M., Trams N. R., Valentijn E. A., Vandenbussche B., van den Ancker M. E., van Dishoeck E. F., van Winckel H., Wesselius P. R., and Young E. T. (1996) Mineralogy of oxygen-rich dust shells. *Astron. Astrophys.* **315**, L361-L364.

Watts J. F. and Wolstenholme J. (2003) *An Introduction to Surface Analysis by XPS and AES*. John Wiley and Sons Ltd. 212 pp.

Yada T., Stadermann F. J., Floss C., Zinner E., Olinger C. T., Graham G. A., Bradley J. P., Dai Z., Nakamura T., Noguchi T., and Bernas M. (2005) Discovery of abundant presolar silicates in subgroups of Antarctic micrometeorites. *Lunar Planet. Sci. XXXVI*, #1227.

Zinner E. (2004) Presolar grains. In *Meteorites, Planets and Comets*, A. M. Davis, Ed. (Vol. 1, Treatise on Geochemistry, H. D. Holland, K. K. Turekian, Exec. Eds.) pp. 17-39. Elsevier Science.

Zinner E., McKeegan K. D., and Walker R. M. (1983) Laboratory measurements of D/H ratios in interplanetary dust. *Nature* **305**, 119-121.

Zinner E., Ming T., and Anders E. (1989) Interstellar SiC in the Murchison and Murray meteorites: isotopic composition of Ne, Xe, Si, C, and N. *Geochim. Cosmochim. Acta* **53**, 3273-3290.

Zinner E., Amari S., Wopenka B., and Lewis R. S. (1995) Interstellar graphite in meteorites: isotopic compositions and structural properties of single graphite grains from Murchison. *Meteoritics* **30**, 209-226.

Ziurys L. M., Savage C., Brewster M. A., Apponi A. J., Pesch T. C., and Wyckoff S. (1999) Cyanide chemistry in comet Hale-Bopp (C/1995 O1). *Astrophys. J.* **527**, L67-L71.

Table 1. Interplanetary dust particles measured in this study

Name*	Particle designation	Size (μm^2)§	Composition†	Measurements#
Prudhomme	L2009-N2	10 x 10	c-type	H-3f, C, N
Maeterlinck	L2009-N10	15 x 10	c-type	C, N, O
Hamsun	L2009-N11	10 x 10	c-type	H, B, C, N, O
Bergson	L2009-c5-H2	10 x 8	c-type	H, B, C, N, O
Anatole	L2009-c5-H3	12 x 9	c-type	H, B, C, N, O
O'Neill	L2009-c13-I2	12 x 10	c-type, S-rich	H, B, C, N, O, S
Mommsen	L2009-c13-I3	13 x 12	c-type, pyroxene?	H-3f, *C, N*
du Gard	L2009-c13-I4	10 x 10	c-type	H, B, C, N, O, S
Bjornson	L2011-Q2	10 x 10	c-type, S-rich	H-3f
Kipling	L2011-R12	12 x 12	c-type	H-3f, C, N, O
Hauptmann	L2011-S12	10 x 10	c-type	*C, N*, O
Lewis	L2011-Z6	12 x 12	c-type, S-rich	O, S
Russell	L2011-c3-AD2	5 x 5	c-type	H-3f, *C, N*
Lagerkvist	L2011-c5-AD6	8 x 8	c-type	H-3f, C, N
Laxness	L2011-c5-AD7	8 x 8	c-type	H-3f
Faulkner	L2011-c6-AD8	10 x 10	c-type	H-3f, *C, N*
Pasternak	L2011-c8-AD13	7 x 7	c-type, olivine?	H-3f, *C, N*
Mauriac	L2011-c8-AD14	7 x 7	c-type	H-3f, C, N
Gjellerup	L2011-c11-D2	14 x 13	c-type	C, N, O
Sillanpää	L2011-c11-D3	12 x 12	c-type	H, B, C, N, O, S
Jiménez	L2011-c17-AD19	5 x 5	c-type	C, N
Hemingway	L2011-c17-AD20	5 x 5	c-type, olivine?	H-3f, C, N
Mistral F.	L2036-E6	9 x 9	c-type	H-3f, C, N
Echegaray	L2036-F18	14 x 14	c-type	H-3f, *C, N*
Rolland	L2036-F19	16 x 15	c-type	*C, N*, O
Benavente	L2036-G16	10 x 10	c-type	C, N, O
Yeats	L2036-I19	12 x 12	c-type	H, B, C, N, O
von Heidenstam	L2036-I27	16 x 10	c-type	*C, N*, O
Reymont	L2036-c9-D2	13 x 12	c-type	H, B, C, N, O
Sienkiewicz	L2036-c9-D3	14 x 13	c-type	H-3f, C, N
Carducci	L2036-c14-G3	15 x 12	c-type	H-3f, *C, N*
Eucken	L2036-c17-E2	13 x 12	c-type	H-3f, *C, N*
Jensen	L2036-c17-E3	11 x 10	c-type, pyroxene?	H, B, C, N, O, S
Shaw	L2036-c17-E4	14 x 12	c-type	H, B, C, N, O
Galsworthy	L2036-c18 F2	8 x 8	c-type	H, B, C, N, O, S
Mistral G.	L2036-c18-F3	9 x 9	c-type, S-rich	H, B, C, N, O, S
Hesse	L2036-c18-F4	8 x 7	c-type	H, B, C, N, O, S
Gide	L2036-c21-H2	9 x 8	c-type	H, B, C, N, O, S
Deledda	L2036-c21-H3	9 x 8	c-type	H, B, C, N, O
Bunin	L2036-c21-H4	13 x 12	c-type, S-rich	H, B, C, N, O, S
Eliot	L2036-c24-I3	9 x 8	c-type	C, N, O, S
Pirandello	L2036-c24-I4	9 x 8	c-type	H, B, C, N, O, S

*IDPs are nicknamed after winners of the Nobel Prize for Literature; §refers to original size before pressing into Au foil; †c-type particles defined by Stadermann (1991); some IDPs appear to be dominated by a particular phase or element, as indicated; see text for details. #H-3f indicates H measurements made with the ims 3f, all other measurements were made with the NanoSIMS; italics indicate a measurement was made, but no statistically significant results were obtained.

Table 2. Hydrogen isotopic compositions in IDPs*

Name	Particle designation	δD_{SMOW} (‰)
Prudhomme	L2009-N2	305 ± 101
		248 ± 90
Mommsen	L2009-c13-I3	-84 ± 76
Bjornson	L2011-Q2	125 ± 104
		+29 ± 89
Kipling	L2011-R12	467 ± 122
		945 ± 142
		722 ± 126
		752 ± 127
		748 ± 140
Russell	L2011-c3-AD2	3593 ± 495
		385 ± 254
Lagerkvist	L2011-c5-AD6	-173 ± 69
		-106 ± 52
		120 ± 66
Laxness	L2011-c5-AD7	87 ± 59
		-70 ± 63
Faulkner	L2011-c6-AD8	862 ± 107
		220 ± 93
Pasternak	L2011-c8-AD13	-253 ± 160
		–64 ± 211
Mauriac	L2011-c8-AD14	535 ± 336
Hemingway	L2011-c17-AD20	192 ± 84
Mistral F.	L2036-E6	-197 ± 66
		-315 ± 56
		-239 ± 55
Echegaray	L2036-F18	460 ± 169
		112 ± 86
		173 ± 108
Sienkiewicz	L2036-c9-D3	278 ± 100
		58 ± 80
Carducci	L2036-c14-G3	-7 ± 96
Eucken	L2036-c17-E2	-512 ± 39
		-58 ± 79

*measurements made with the ims 3f; errors are 1σ.

Table 3. Carbon and nitrogen isotopic compositions in IDPs

Name*	Particle Designation	Area	$^{12}C/^{13}C$	$\delta^{13}C$ (‰)	$^{14}N/^{15}N$	$\delta^{15}N$ (‰)	Size (nm^2)
Prudhomme	L2009-N2	bulk	89.4 ± 3.4	7 ± 38	234.6 ± 4.5	160 ± 22	
Maeterlinck	L2009-N10	bulk	92.7 ± 1.7	-29 ± 18	258.7 ± 6.0	51 ± 24	
Hamsun	L2009-N11	bulk	89.2 ± 1.5	9 ± 17	267.8 ± 2.2	16 ± 9	
		hotspot 1	89.5 ± 11.8	6 ± 133	145.9 ± 6.9	864 ± 88	685 x 685
Bergson	L2009-c5-H2	bulk	87.4 ± 1.1	30 ± 13	272.7 ± 2.6	-3 ± 10	
Anatole	L2009-c5-H3	bulk	93.8 ± 3.7	-41 ± 37	257.3 ± 7.7	57 ± 32	
O'Neill	L2009-c13-I2	bulk	86.6 ± 1.5	39 ± 19	250.6 ± 2.4	85 ± 11	
		hotspot 1	85.9 ± 2.5	48 ± 31	132.2 ± 3.5	1057 ± 55	235 x 235
		hotspot 2	81.4 ± 3.6	106 ± 49	150.0 ± 5.8	813 ± 70	235 x 235
du Gard	L2009-c13-I4	bulk	89.7 ± 1.6	3 ± 18	250.2 ± 2.4	87 ± 11	
		hotspot 1	85.7 ± 2.5	50 ± 31	134.5 ± 4.6	1022 ± 69	340 x 340
		hotspot 2	87.5 ± 2.2	29 ± 26	146.5 ± 2.4	857 ± 30	585 x 685
Kipling	L2011-R12	bulk	80.5 ± 4.5	118 ± 62	180.7 ± 2.3	505 ± 20	
		hotspot 1	77.7 ± 13.3	158 ± 199	118.1 ± 5.6	1303 ± 109	410 x 340
		hotspot 2	90.8 ± 16.9	-9 ± 184	128.3 ± 5.0	1120 ± 82	545 x 685
Lagerkvist	L2011-c5-AD6	bulk	86.9 ± 9.7	36 ± 115	273.1 ± 8.5	-4 ± 31	
Mauriac	L2011-c8-AD14	bulk	82.1 ± 4.5	96 ± 60	269.2 ± 9.1	10 ± 34	
Gjellerup	L2011-c11-D2	bulk	88.2 ± 0.8	20 ± 9	251.1 ± 1.5	83 ± 6	
		hotspot 1	87.1 ± 4.0	33 ± 47	163.6 ± 6.1	663 ± 62	350 x 350
Sillanpää	L2011-c11-D3	bulk	89.9 ± 1.3	1 ± 15	245.1 ± 2.9	110 ± 13	
		hotspot 1	81.3 ± 5.3	107 ± 73	128.2 ± 11.7	1122 ± 194	295 x 245
Jiménez	L2011-c17-AD19	bulk	82.8 ± 5.0	87 ± 66	271.4 ± 8.3	2 ± 31	
Hemingway	L2011-c17-AD20	bulk	887.0 ± 4.5	34 ± 54	281.7 ± 11.2	-34 ± 38	
Mistral F.	L2036-E6	bulk	90.4 ± 4.6	-4 ± 51	259.8 ± 10.8	47 ± 44	
Benavente	L2036-G16	bulk	90.0 ± 1.0	0 ± 11	232.9 ± 1.7	168 ± 9	
		hotspot 1	93.8 ± 4.4	-41 ± 45	143.0 ± 5.1	902 ± 69	390 x 390
		hotspot 2†	96.6 ± 1.3	-70 ± 13	119.8 ± 1.3	1270 ± 25	800 x 1600
Yeats	L2036-I19	bulk	88.9 ± 1.4	12 ± 16	275.5 ± 2.4	-13 ± 9	
		hotspot 1	82.1 ± 7.7	96 ± 103	137.1 ± 8.3	984 ± 120	295 x 295
Reymont	L2036-c9-D2	bulk	90.2 ± 1.4	-2 ± 16	270.9 ± 6.1	4 ± 23	
		hotspot 1	99.8 ± 5.2	-98 ± 47	165.3 ± 8.4	645 ± 83	295 x 295
Sienkiewicz	L2036-c9-D3	bulk	94.4 ± 5.7	-47 ± 58	263.3 ± 9.0	33 ± 35	
Jensen	L2036-c17-E3	bulk	89.6 ± 1.6	4 ± 18	271.2 ± 2.6	3 ± 10	
Shaw	L2036-c17-E4	bulk	88.5 ± 1.2	17 ± 14	274.0 ± 1.9	-7 ± 7	
Galsworthy	L2036-c18 F2	bulk	89.0 ± 0.7	11 ± 8	223.5 ± 1.2	217 ± 7	
		hotspot 1	86.4 ± 1.8	42 ± 22	134.9 ± 2.4	1016 ± 36	340 x 295
		hotspot 2	86.3 ± 1.0	43 ± 12	135.3 ± 1.2	1010 ± 17	340 x 340
Mistral G.	L2036-c18-F3	bulk	89.8 ± 1.6	2 ± 18	255.9 ± 2.5	63 ± 11	
		hotspot 1	86.6 ± 3.8	39 ± 46	155.2 ± 7.8	753 ± 89	340 x 295
		hotspot 2	86.8 ± 3.7	37 ± 45	161.4 ± 5.6	685 ± 59	295 x 295
Hesse	L2036-c18-F4	bulk	87.1 ± 1.6	33 ± 18	201.7 ± 1.9	349 ± 13	
		hotspot 1	83.9 ± 2.0	73 ± 25	125.3 ± 2.5	1170 ± 43	390 x 390
		hotspot 2	77.4 ± 1.8	163 ± 27	137.9 ± 3.5	972 ± 50	245 x 390
		hotspot 3	91.0 ± 2.1	-11 ± 23	143.3 ± 2.7	898 ± 36	245 x 245
Gide	L2036-c21-H2	bulk	87.1 ± 1.6	33 ± 18	252.0 ± 6.4	79 ± 27	
Deledda	L2036-c21-H3	bulk	89.0 ± 1.0	11 ± 11	221.5 ± 1.7	228 ± 9	
		hotspot 1	87.2 ± 2.2	32 ± 26	167.5 ± 5.1	624 ± 50	625 x 390
Bunin	L2036-c21-H4	bulk	89.3 ± 0.5	8 ± 6	245.5 ± 1.1	108 ± 5	
		hotspot 1	86.3 ± 1.6	43 ± 19	169.4 ± 3.6	606 ± 34	350 x 295
Eliot	L2036-c24-I3	bulk	88.8 ± 1.6	14 ± 18	305.1 ± 3.0	-108 ± 9	
Pirandello	L2036-c24-I4	bulk	89.9 ± 1.3	1 ± 15	267.7 ± 3.4	16 ± 13	
		hotspot 1	89.3 ± 1.8	8 ± 20	146.9 ± 2.8	852 ± 35	390 x 315
		hotspot 2	85.7 ± 1.7	50 ± 21	171.0 ± 3.8	591 ± 36	550 x 315

*isotopically primitive IDPs are highlighted in bold, see text for details; †data from Floss et al. (2004); errors are 1σ.

Table 4. Oxygen isotopic compositions of presolar grains in IDPs*

Name	Particle Designation	Grain	Size (nm^2)	$^{16}O/^{17}O$	$\delta^{17}O$ (‰)	$^{16}O/^{18}O$	$\delta^{18}O$ (‰)
du Gard	L2009-c13-I4	dG1	300 x 300	1782 ± 68	473 ± 56	526 ± 12	-51 ± 22
Kipling	L2011-R12	K1	340 x 480	1229 ± 55	1136 ± 96	491 ± 14	16 ± 29
Benavente	L2036-G16	B1	390 x 390	1081 ± 37	1428 ± 83	496 ± 12	6 ± 24
Galsworthy	L2036-c18-F2	G1	350 x 350	2074 ± 77	266 ± 47	382 ± 6	306 ± 21
		G2	300 x 350	1226 ± 30	1141 ± 52	570 ± 10	-125 ± 15
		G3	200 x 440	702 ± 24	2739 ± 128	717 ± 24	-304 ± 23
Hesse	L2036-c18-F4	H1	300 x 245	1585 ± 78	656 ± 81	460 ± 13	85 ± 31
		H2	245 x 245	2428 ± 185	81 ± 82	318 ± 9	569 ± 44
Deledda	L2036-c21-H3	D1	195 x 155	1649 ± 107	592 ± 103	520 ± 19	-40 ± 35
Eliot	L2036-c24-I3	E1	550 x 700	2262 ± 54	160 ± 28	403 ± 4	238 ± 12

*errors are 1σ.

Table 5. Hydrogen isotopic compositions in IDPs*

Name	Particle Designation	Average Bulk D (δD_{SMOW}, ‰)	D Hotspots (δD_{SMOW}, ‰)	Size (nm^2)	Regional D Variations†
Hamsun	L2009-N11	-45 ± 35	865 ± 180	550 x 550	no
Bergson	L2009-c5-H2	110 ± 25	2785 ± 430	625 x 780	yes
Anatole	L2009-c5-H3	65 ± 35	2335 ± 245	470 x 470	yes
O'Neill	L2009-c13-I2	-80 ± 45	—		no
du Gard	L2009-c13-I4	110 ± 55	2234 ± 445	410 x 410	yes
Sillanpää	L2011-c11-D3	85 ± 55	5095 ± 905	410 x 410	yes
			4370 ± 775	350 x 350	
			2010 ± 350	530 x 530	
Yeats	L2036-I19	150 ± 25	3205 ± 355	585 x 585	yes
Reymont	L2036-c9-D2	120 ± 35	2030 ± 475	470 x 470	no
Jensen	L2036-c17-E3	-10 ± 50	—		no
Shaw	L2036-c17-E4	-25 ± 50	—		no
Galsworthy	L2036-c18 F2	10 ± 65	3200 ± 670	470 x 470	yes
Mistral G.	L2036-c18-F3	-130 ± 45	—		no
Hesse	L2036-c18-F4	225 ± 70	2625 ± 750	350 x 350	no
Gide	L2036-c21-H2	-100 ± 45	—		no
Deledda	L2036-c21-H3	20 ± 25	560 ± 85	700 x 530	no
Bunin	L2036-c21-H4	260 ± 30	3320 ± 405	550 x 550	yes
Pirandello	L2036-c24-I4	60 ± 40	—		no

*NanoSIMS measurements, errors are 1σ; †micron-sized or larger areas that show variable enrichments of D on the order of several hundreds of permil.

FIGURE CAPTIONS

Figure 1. Secondary electron microphotographs of four different IDPs and their corresponding EDX spectra. See text for details of the compositional definitions.

Figure 2. Hydrogen isotopic compositions in IDPs. Shown are D/H ratios, normalized to SMOW (Standard Mean Ocean Water) with each circle representing a different measurement in the same particle, thus illustrating the degree of H isotopic heterogeneity within a given IDP. The shaded region shows the range of terrestrial D/H values (Hoefs, 1980).

Figure 3. Carbon and nitrogen isotopic compositions of a) Bergson and b) Pirandello. Shown are isotope plots of the $^{12}C/^{13}C$ and $^{14}N/^{15}N$ ratios of 500 nm-sized sub-regions of the IDPs and false color images of the $\delta^{13}C$ and $\delta^{15}N$ compositions of the particles. Both IDPs have isotopically normal bulk compositions in C and N, but Pirandello contains two hotspots enriched in ^{15}N. Gray areas indicate regions with insufficient signal for statistically significant analysis. Dashed lines show terrestrial C and N ratios.

Figure 4. Carbon and nitrogen isotopic compositions of a) Hesse and b) Eliot. Shown are isotope plots of the $^{12}C/^{13}C$ and $^{14}N/^{15}N$ ratios of 500 nm-sized sub-regions of the IDPs and false color images of the $\delta^{13}C$ and $\delta^{15}N$ compositions of the particles. Hesse has a bulk composition that is enriched in ^{15}N and contains three hotspots that are enriched in ^{15}N; one of these is also enriched in ^{13}C. Eliot has a bulk composition that is depleted in ^{15}N (^{14}N-rich relative to terrestrial). Gray areas indicate regions with insufficient signal for statistically significant analysis. Dashed lines show terrestrial C and N ratios.

Figure 5. False color images of the IDP Galsworthy showing three isotopically anomalous presolar grains. The upper frames show the $\delta^{17}O$ and $\delta^{18}O$ images and the lower frames show the secondary electron and $^{28}Si^+$ images. Gray areas indicate regions with insufficient signal for statistically significant analysis. The image areas represent 25 x 25 μm^2 each and the presolar grains, labeled G1, G2 and G3, are on the order of 300 nm in diameter.

Figure 6. False color images of the IDP Eliot showing an isotopically anomalous presolar grain. The upper frames show the $\delta^{17}O$ and $\delta^{18}O$ images and the lower frames show the secondary electron and $^{28}Si^+$ images. Gray areas indicate regions with insufficient signal for statistically

significant analysis. The image areas represent 20 x 20 μm^2 each and the presolar grain, labeled E1 is 550 x 700 nm^2 in size.

Figure 7. Three isotope O plot showing the compositions of anomalous grains compared with isotopically normal sub-regions of the IDPs in which they were found. Dashed lines show solar ratios. Errors are 1σ; see Table 4 for the isotopic ratios.

Figure 8. False color images of a) c-type IDP du Gard and b) S-rich IDP O'Neill. The first two frames in each set show the ^{32}S distribution and an SE image of the particle, followed by the S isotopic compositions ($\delta^{34}S$ and $\delta^{33}S$). Gray areas indicate regions with insufficient signal for statistically significant analysis. Image areas are 25 x 25 μm^2 for du Gard and 20 x 20 μm^2 for O'Neill.

Figure 9. False color images showing the H isotopic compositions (δD_{SMOW}) of (a) Bunin and (b) Reymont. Note that smoothing of the images during data processing leads, as well as the larger primary beam diameter during H isotopic measurements, to an increase in the apparent size and a dilution of the composition of small features such as the D hotspots. Gray areas indicate regions with insufficient signal for statistically significant analysis. Images are 20 x 20 μm^2 each.

Figure 10. False color images of the IDP Hamsun showing H isotopic compositions and elemental distributions. The open circle shows a D-rich hotspot that consists primarily of C and N (as CN^-). Gray areas indicate regions with insufficient signal for statistically significant analysis. Note that smoothing of the H isotopic image during data processing, as well as the larger primary beam diameter during H isotopic measurements, leads to an increase in the apparent size of the D hotspot.

Figure 11. CN^-/C^- ratios versus $\delta^{15}N$ (‰) for a) bulk IDPs and b) ^{15}N-rich hotspots within the IDPs. Open circles represent IDPs with anomalous bulk N isotopic compositions and closed circles represent IDPs with normal bulk N isotopic compositions. Note the scale change on the CN^-/C^- axis in (b).

Figure 12. Secondary electron microphotographs of presolar silicate grains. Arrows show the location of each grain. Most grains have a smooth platy appearance, but some (e.g., H2, E1) appear to consist of aggregates of smaller grains.

Figure 13. Secondary electron micrographs showing the preparation of a thin section containing the isotopic anomalous material identified in Eliot from NanoSIMS analyses. a) SE image showing the Pt cap deposited on the surface of Eliot that contained the hotspot using the electron

beam. b) SE image of Eliot after the FIB has been used to mill material away either side of the region of interest. c) SE image of Eliot after the region of interest has been extracted and mounted onto a Cu grid and been thinned to approximately 100nm thick.

Figure 14. Bright field images of the TEM section of presolar grain E1 from Eliot showing the presence of multiple GEMS regions. The white inset box in the image on the left shows the region magnified on the right. Circles show the locations of EDX analyses of two Mg-rich areas. The Cu and Ga, Cs and Au peaks in the spectra are contaminants from the FIB technique, the SIMS beam and Au substrate, respectively.

Figure 15. Scanning Auger microprobe images of presolar grain D1 from IDP Deledda. a) SE image; b) composite RGB Auger image (red = Ca, green = Fe, blue = Mg). The grain, shown in the center of the white circles, is about 160 nm in diameter and is an Fe-rich silicate. Image areas are 9 x 12 μm^2.

Figure 1

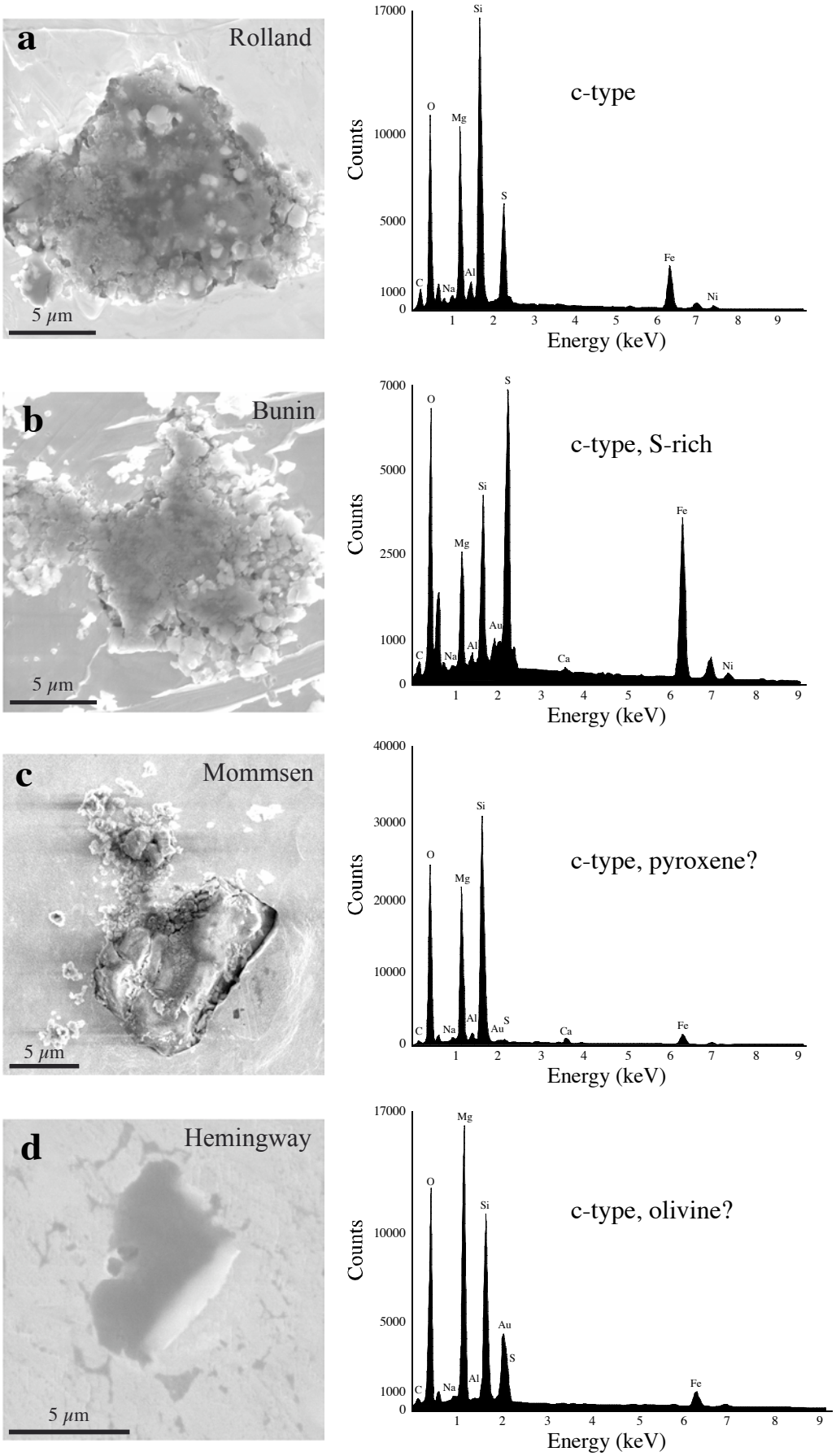
a
Rolland
5 μm
c-type
Counts
Energy (keV)
b
Bunin
5 μm
c-type, S-rich
c
Mommsen
5 μm
c-type, pyroxene?
d
Hemingway
5 μm
c-type, olivine?

Figure 2

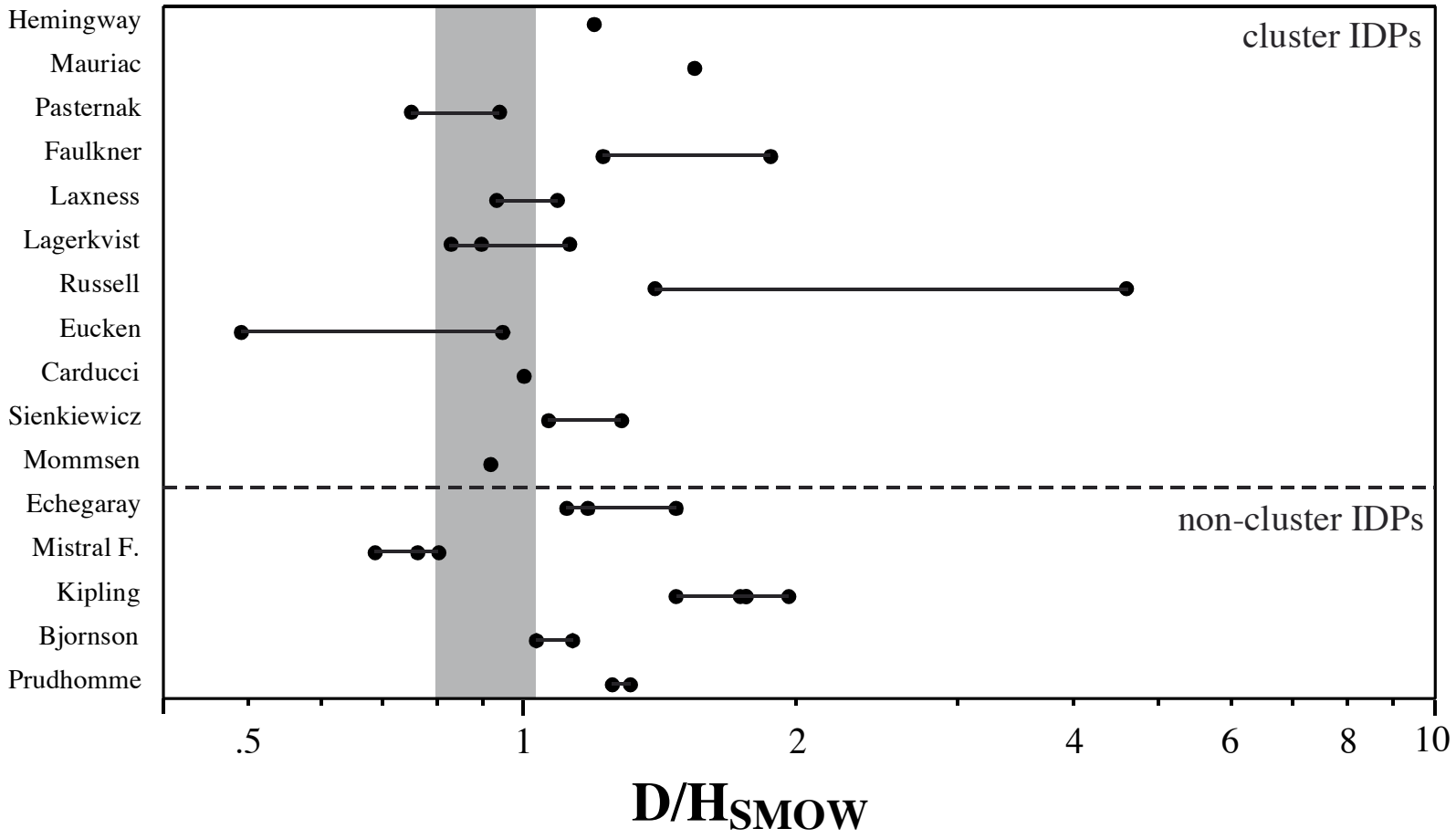
Hemingway
Mauriac
Pasternak
Faulkner
Laxness
Lagerkvist
Russell
Eucken
Carducci
Sienkiewicz
Mommsen
Echegaray
Mistral F.
Kipling
Bjornson
Prudhomme
cluster IDPs
non-cluster IDPs
.5
1
2
4
6
8
10
D/H$_{SMOW}$

Figure 3a

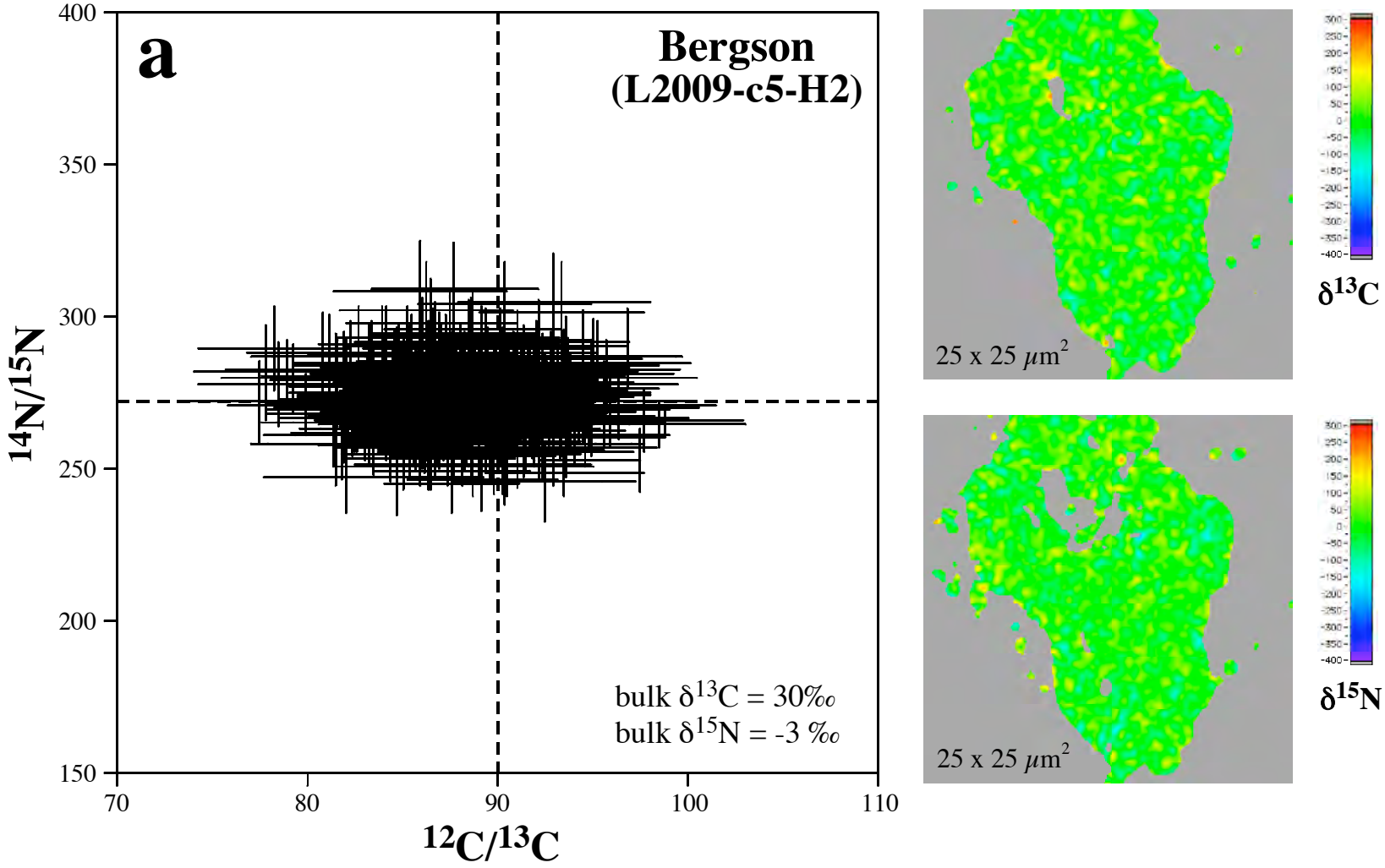
a
Bergson
(L2009-c5-H2)
400
350
300
250
200
150
70
80
90
100
110
14N/15N
12C/13C
bulk δ13C = 30‰
bulk δ15N = -3 ‰
25 x 25 μm2
δ13C
25 x 25 μm2
δ15N

Figure 3b

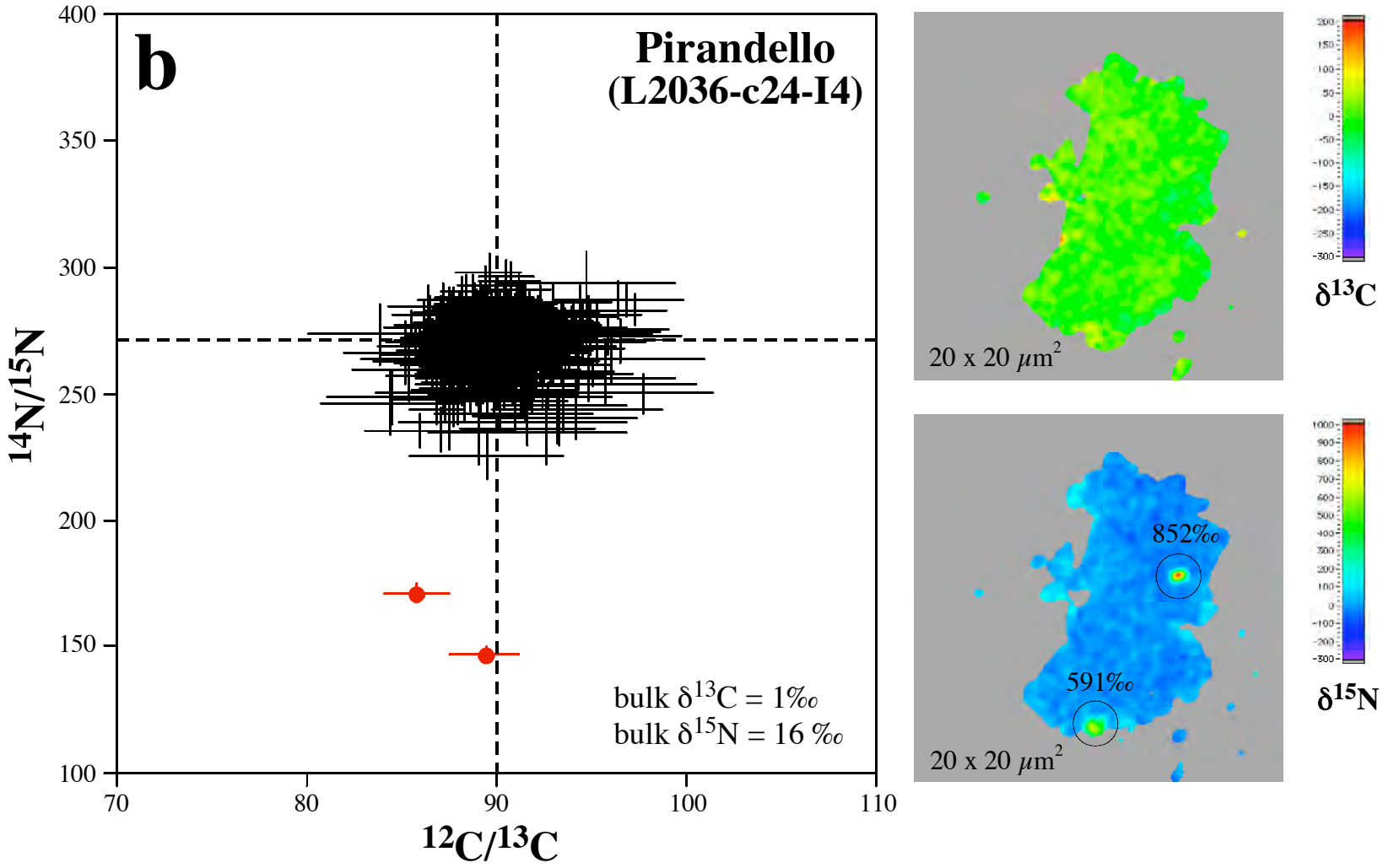
b
Pirandello
(L2036-c24-I4)
400
350
300
250
200
150
100
70
80
90
100
110
14N/15N
12C/13C
bulk δ13C = 1‰
bulk δ15N = 16 ‰
20 x 20 μm2
δ13C
852‰
591‰
20 x 20 μm2
δ15N

Figure 4a

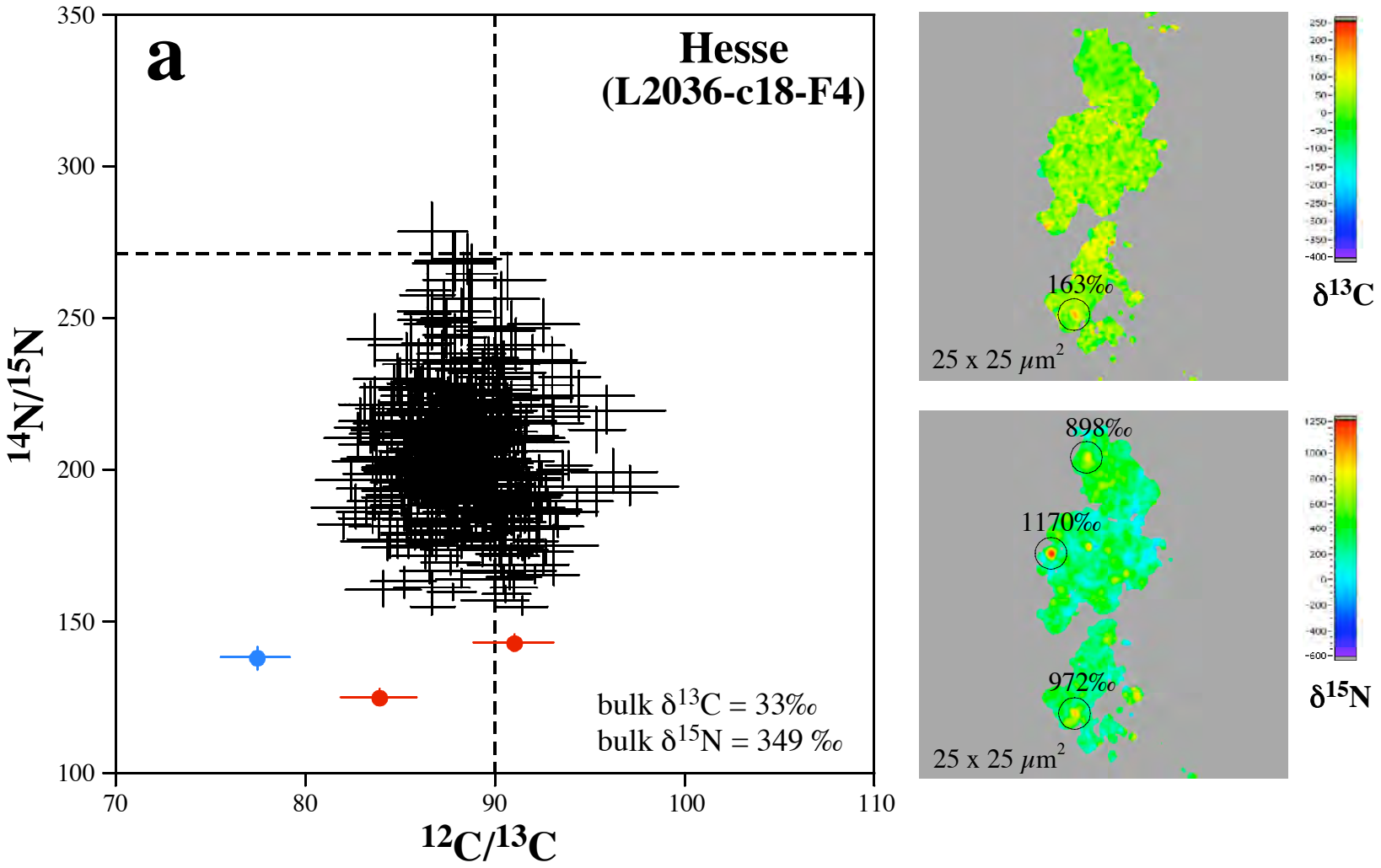
a
Hesse
(L2036-c18-F4)
350
300
250
200
150
100
70
80
90
100
110
14N/15N
12C/13C
bulk δ13C = 33‰
bulk δ15N = 349 ‰
163‰
25 x 25 μm2
δ13C
898‰
1170‰
972‰
25 x 25 μm2
δ15N

Figure 4b

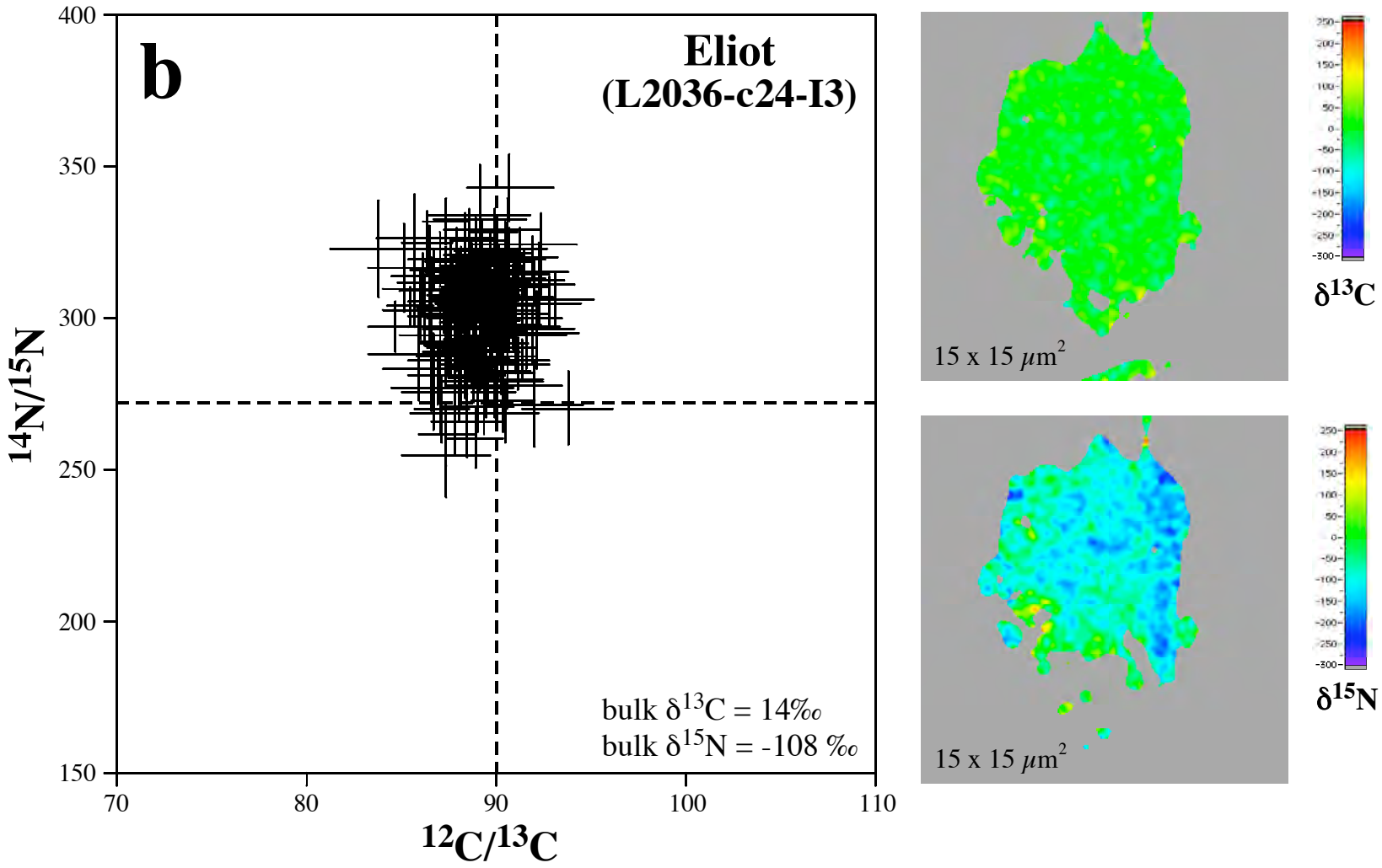
b
Eliot
(L2036-c24-I3)
400
350
300
250
200
150
70
80
90
100
110
14N/15N
12C/13C
bulk δ13C = 14‰
bulk δ15N = -108 ‰
15 x 15 μm2
δ13C
15 x 15 μm2
δ15N

Figure 5

Galsworthy (L2036-c18-F2)

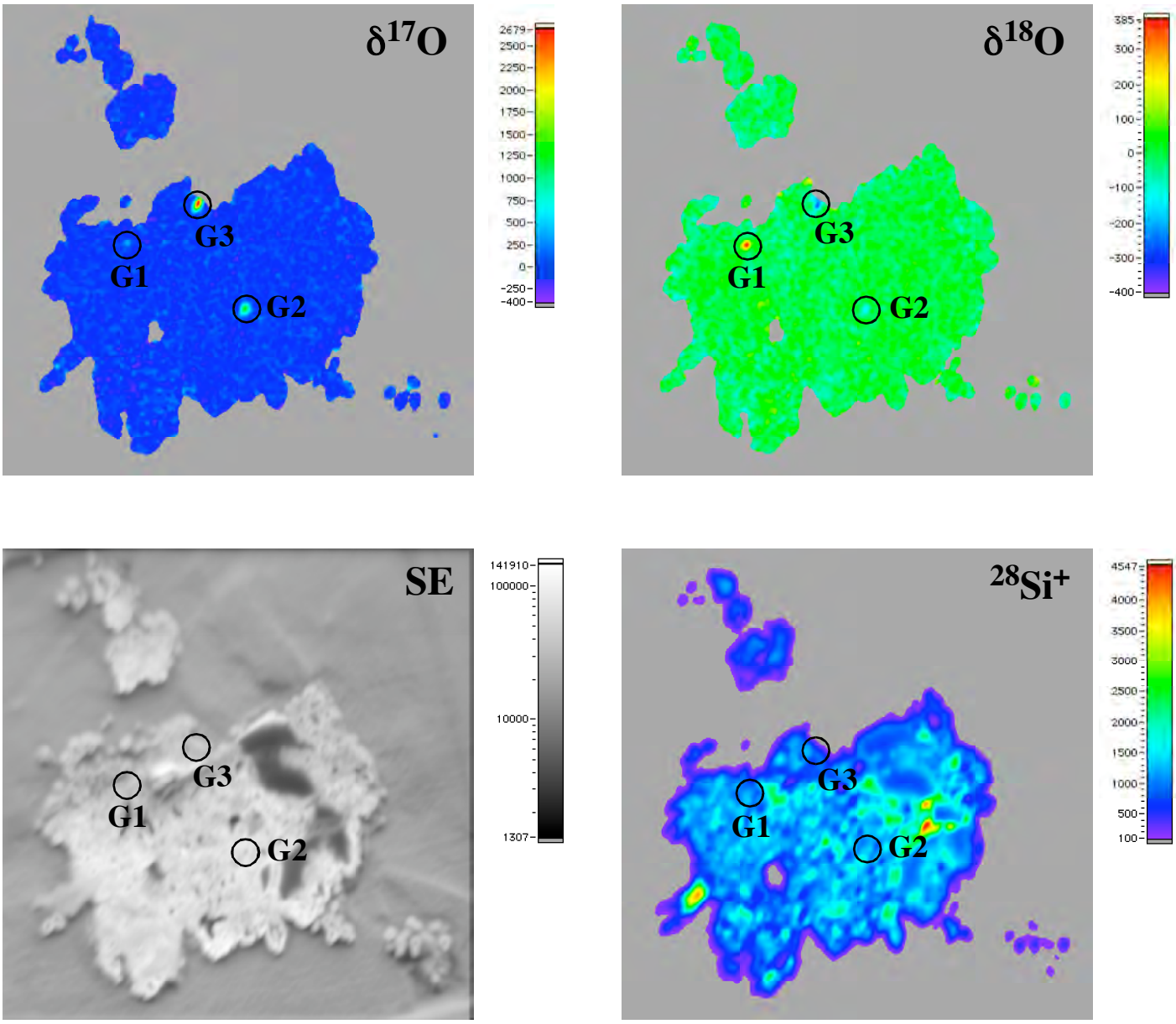

Figure 6

Eliot (L2036-c24-I3)

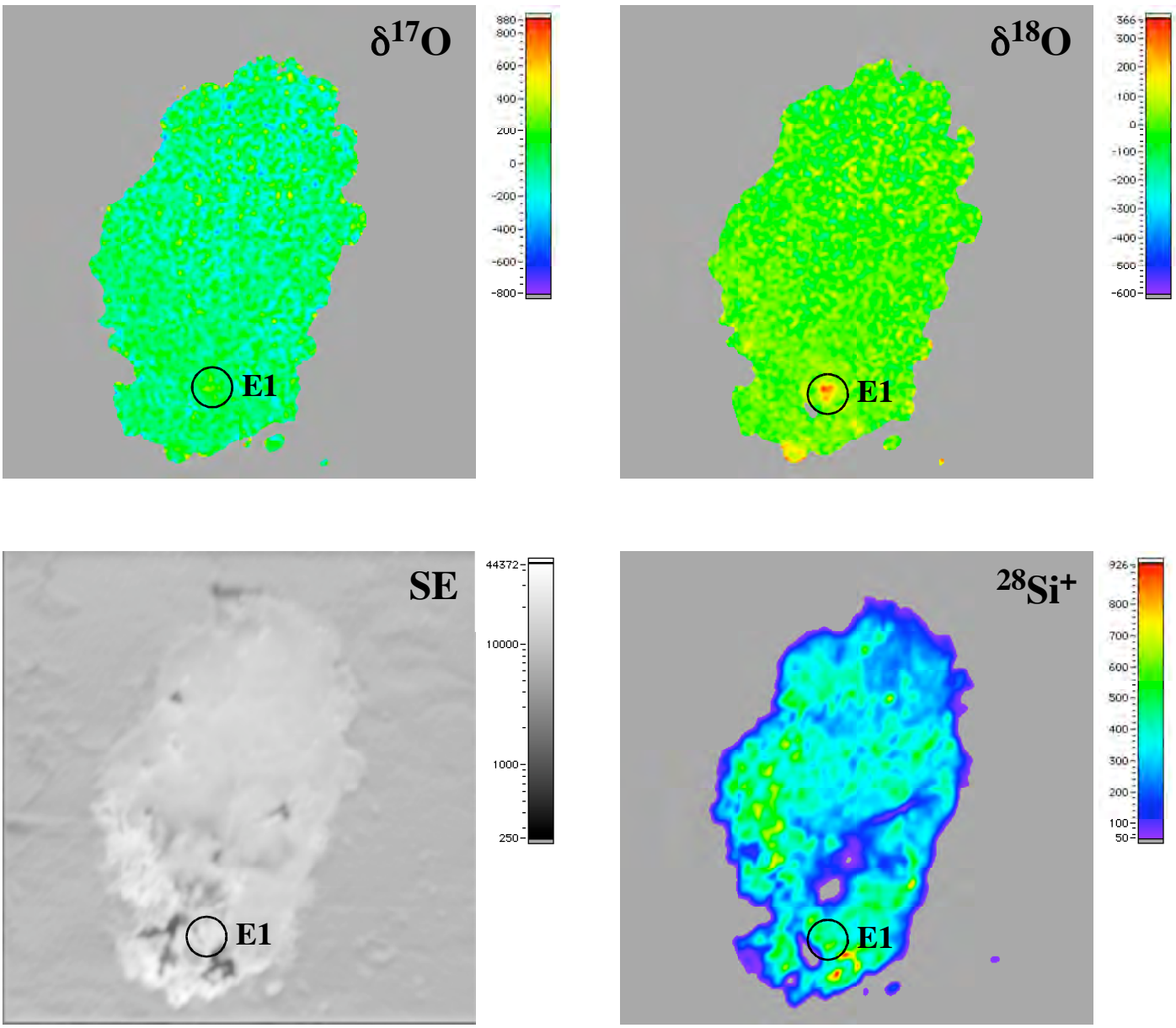

Figure 7

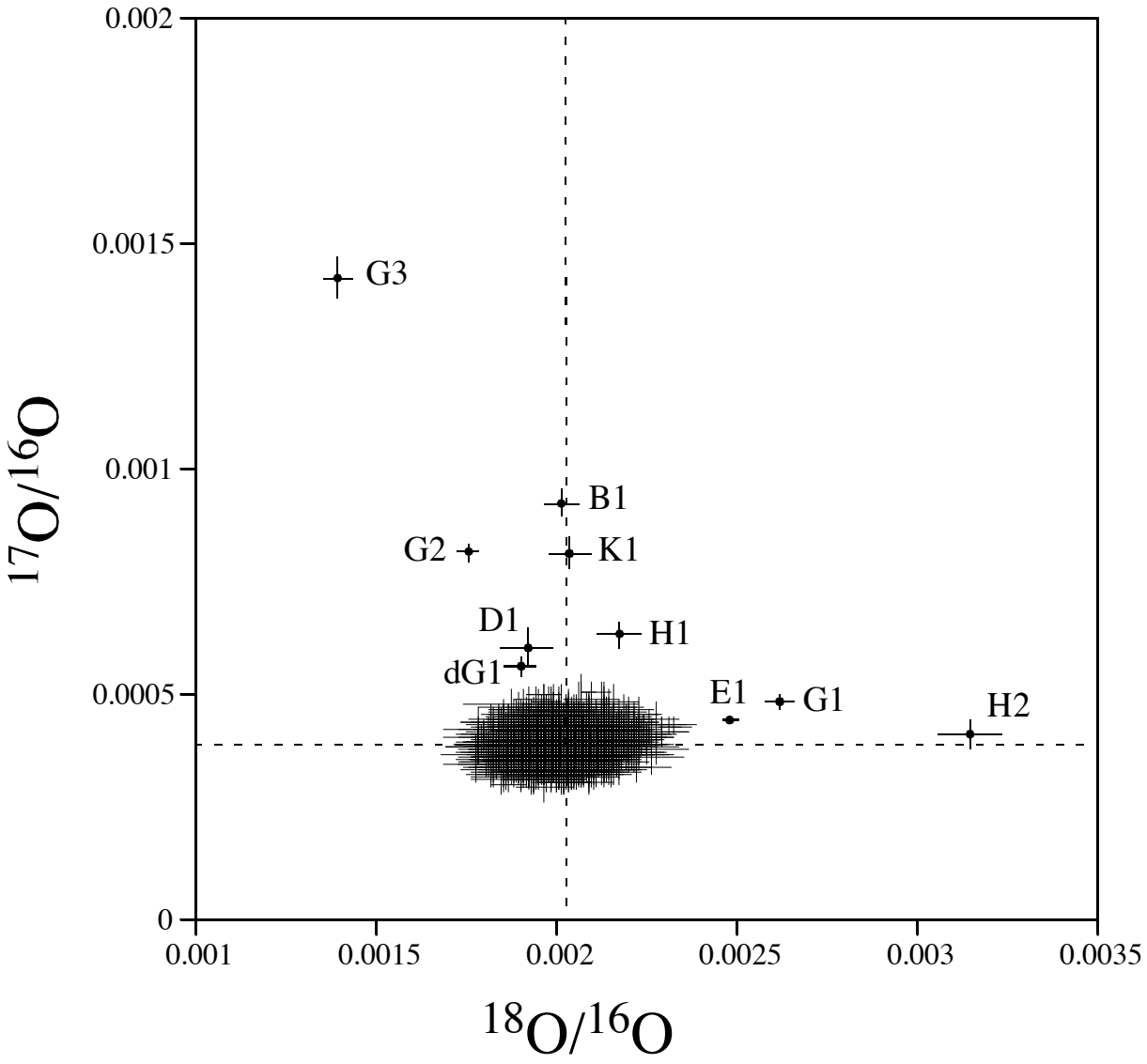
0.002
0.0015
0.001
0.0005
0
0.001
0.0015
0.002
0.0025
0.003
0.0035
$^{17}O/^{16}O$
$^{18}O/^{16}O$
G3
B1
G2
K1
D1
H1
dG1
E1
G1
H2

Figure 8

a) du Gard (L2009-c13-I4)

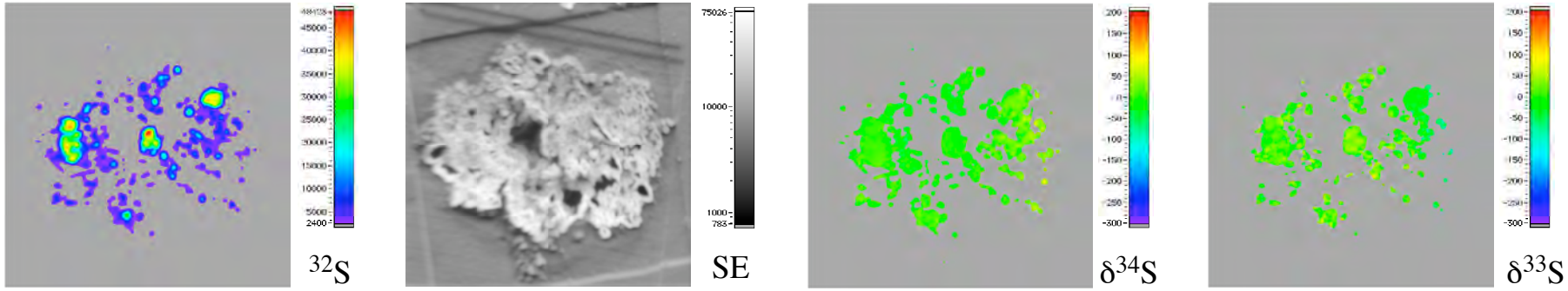

b) O'Neill (L2009-c13-I2)

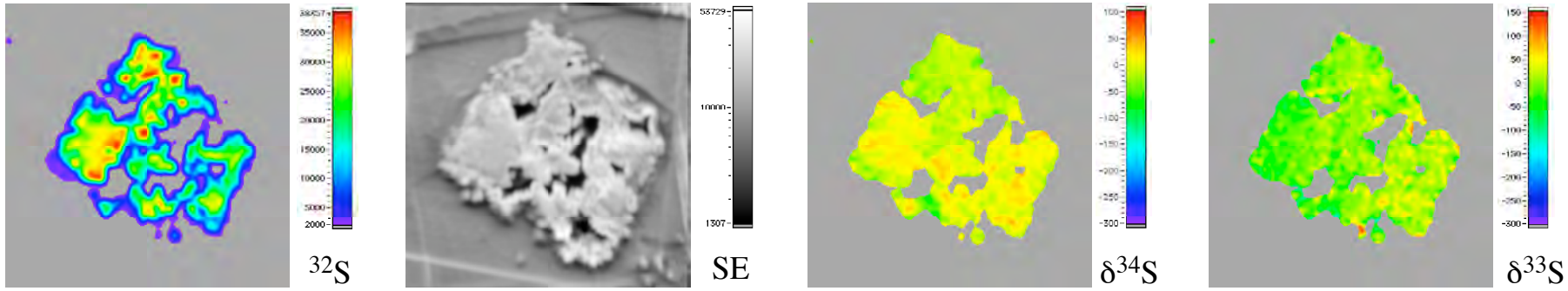

Figure 9

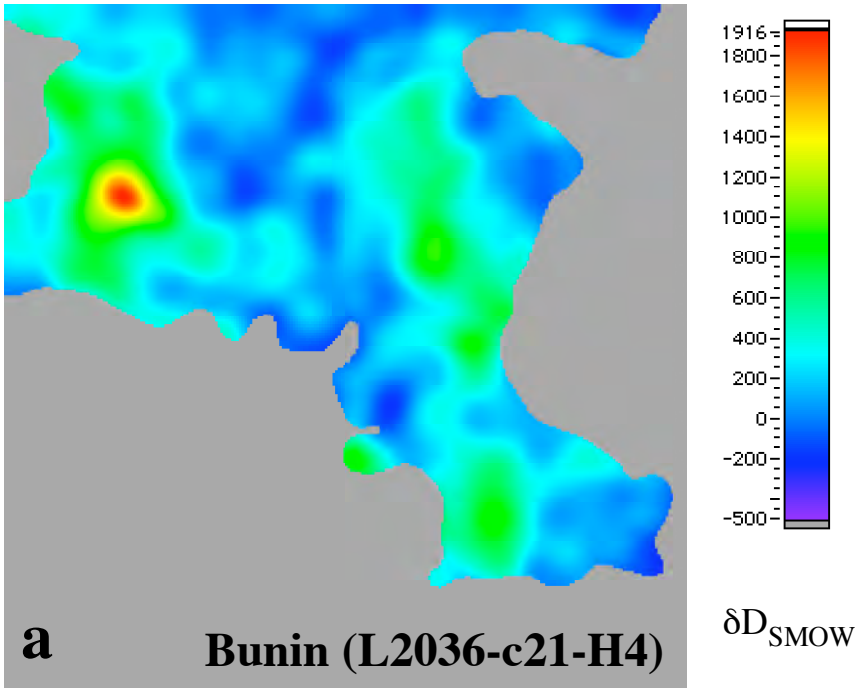

δD_{SMOW}

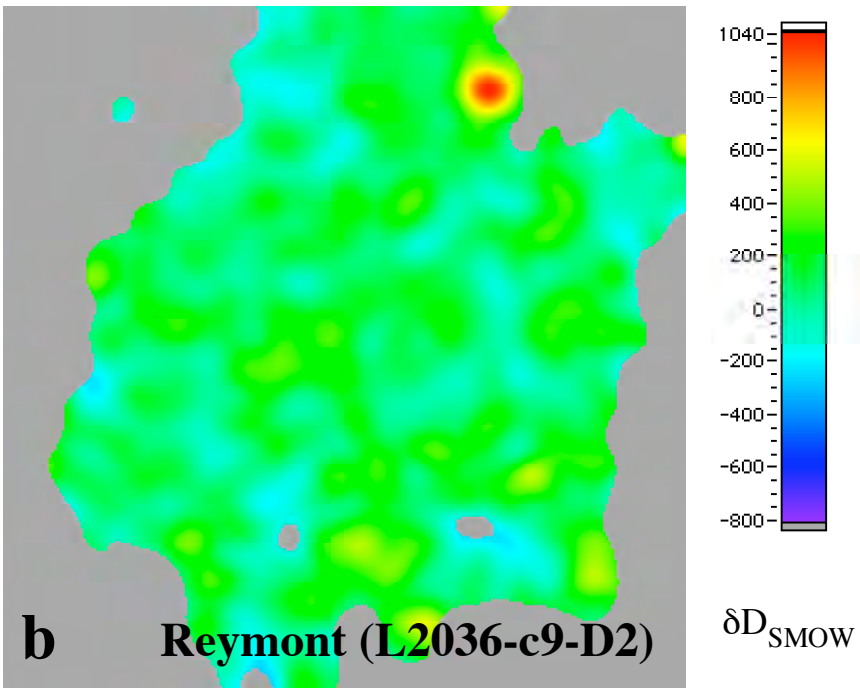

δD_{SMOW}

Figure 10

Hamsun (L2009-N11)

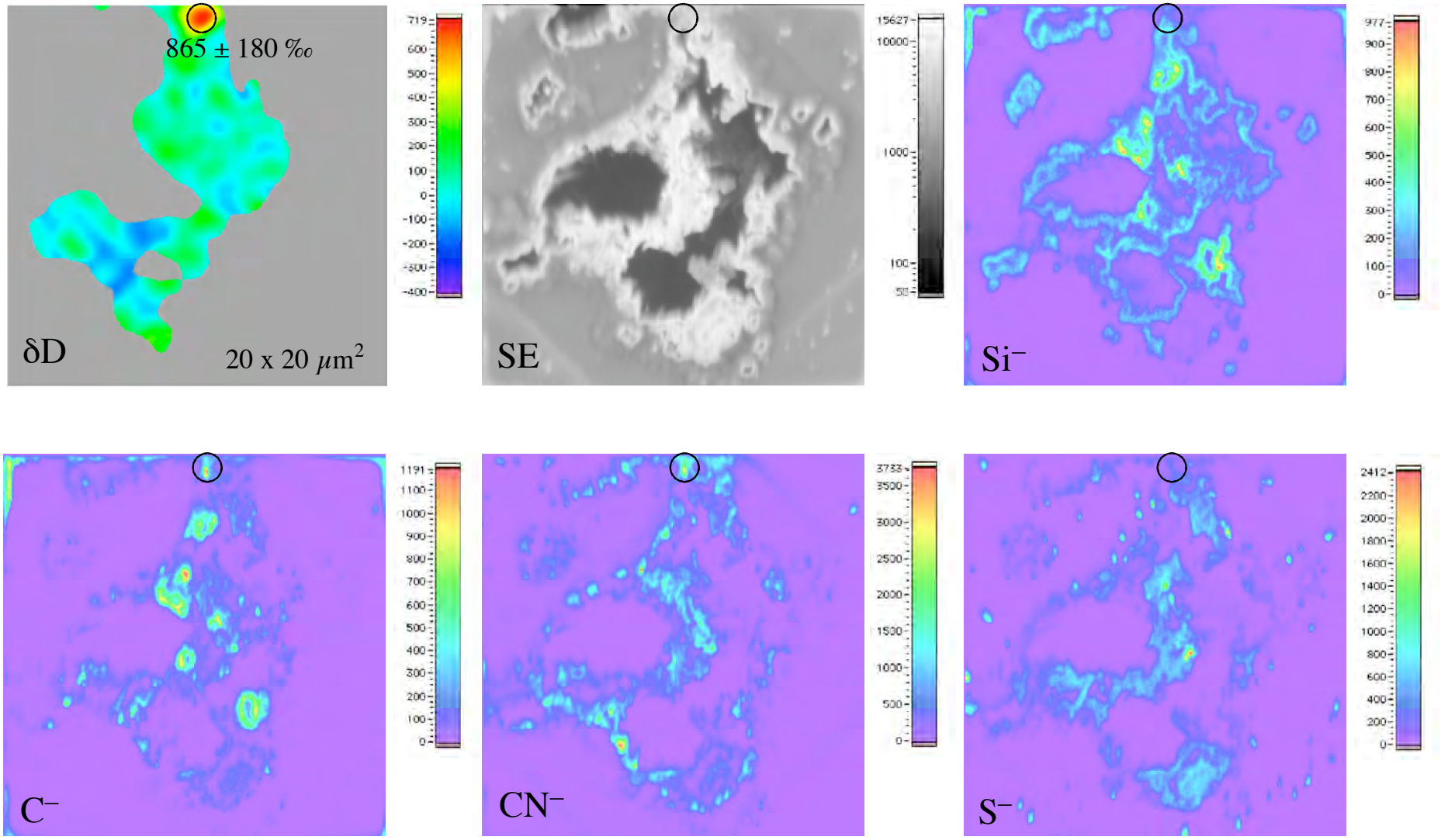

Figure 11

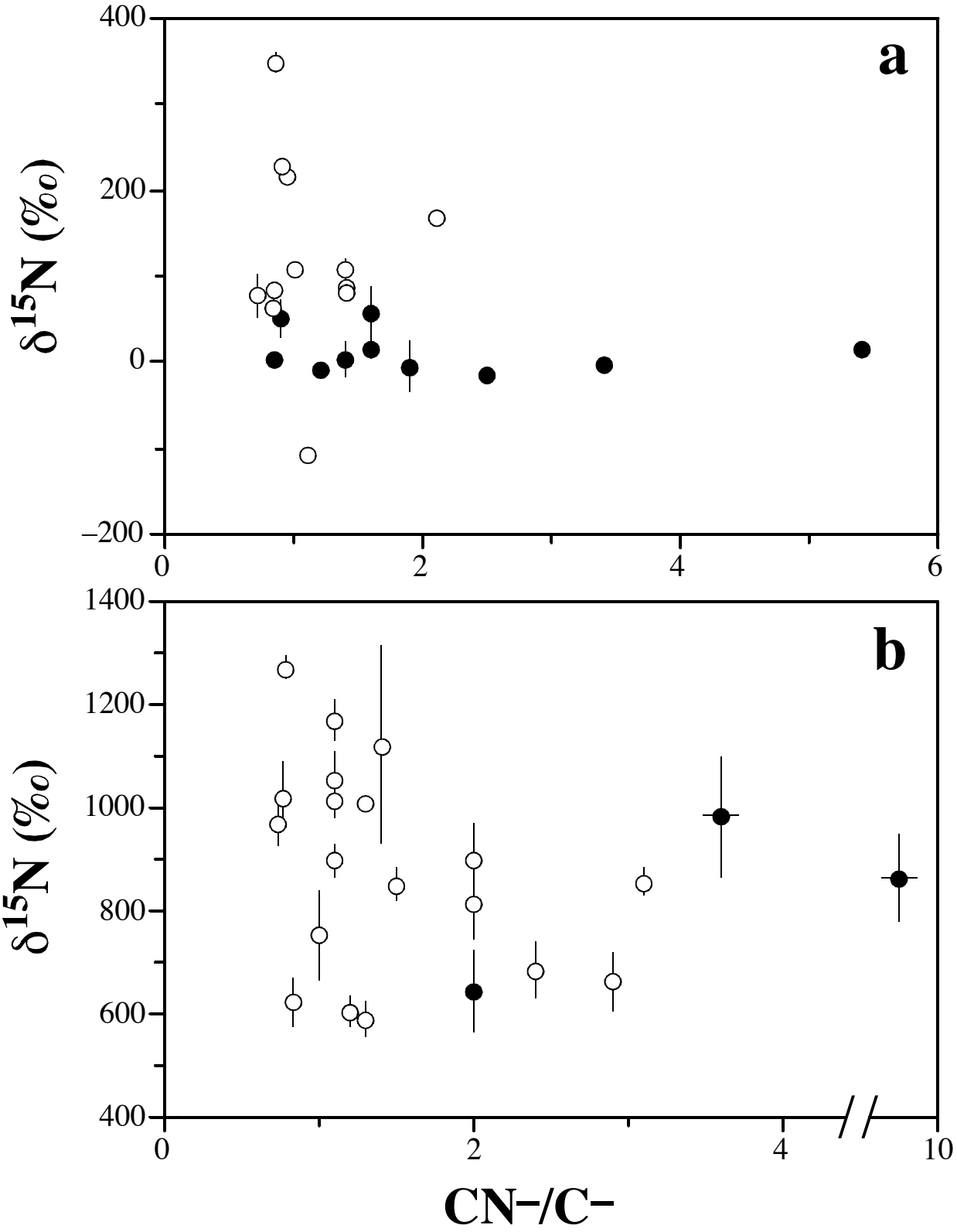
a
b
400
200
0
–200
1400
1200
1000
800
600
400
0
2
4
6
10
δ15N (‰)
δ15N (‰)
CN–/C–

Figure 12

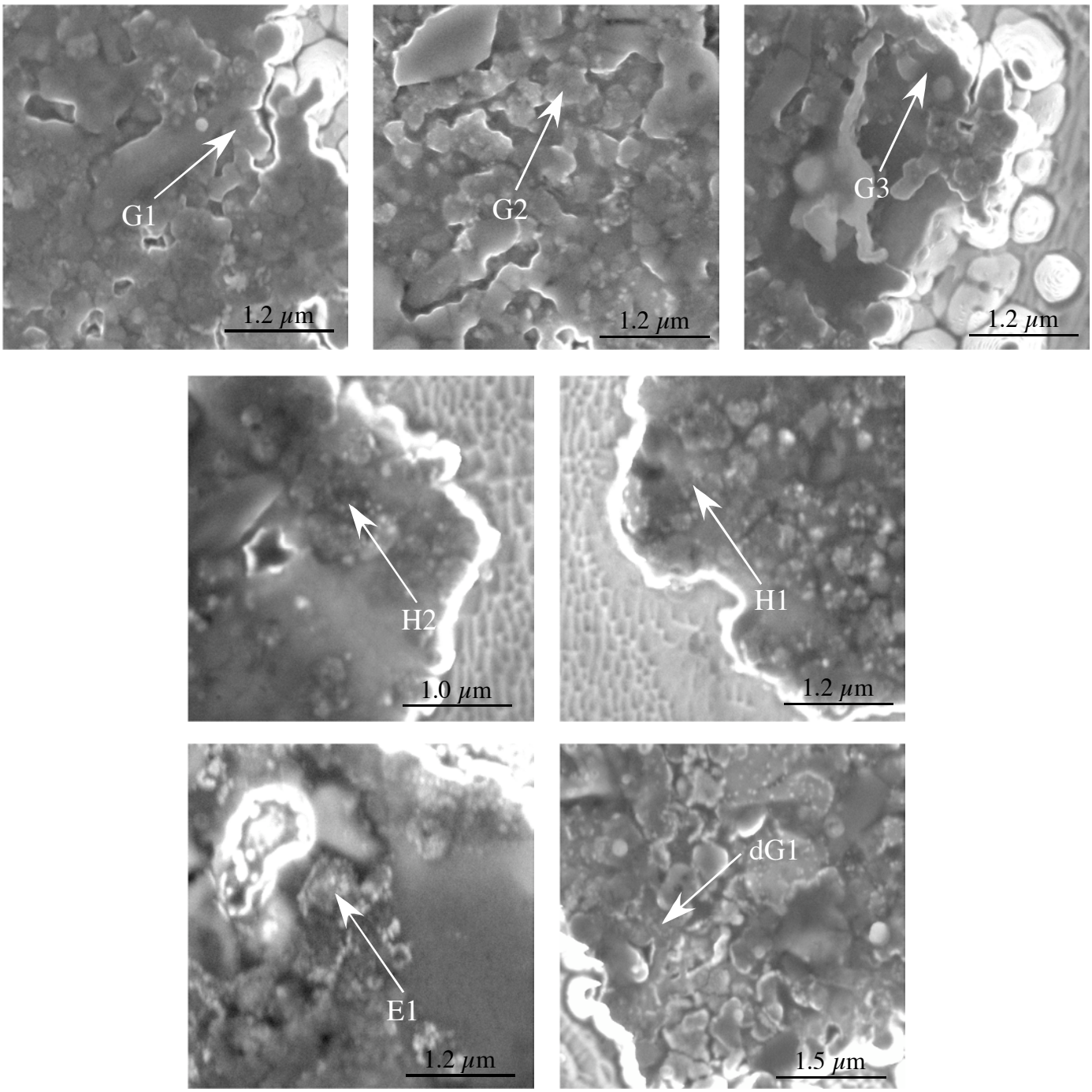

Figure 13

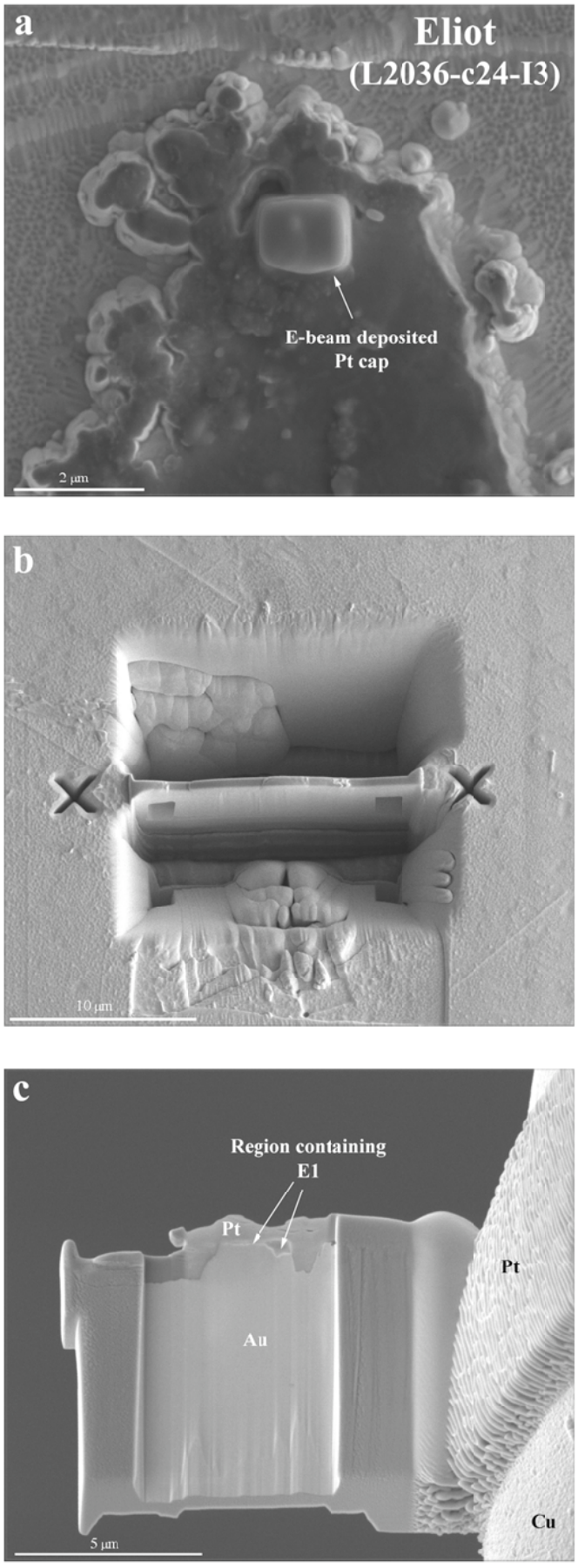
a
Eliot
(L2036-c24-I3)
E-beam deposited
Pt cap
2 μm
b
10 μm
c
Region containing
E1
Pt
Pt
Au
Cu
5 μm

Figure 14

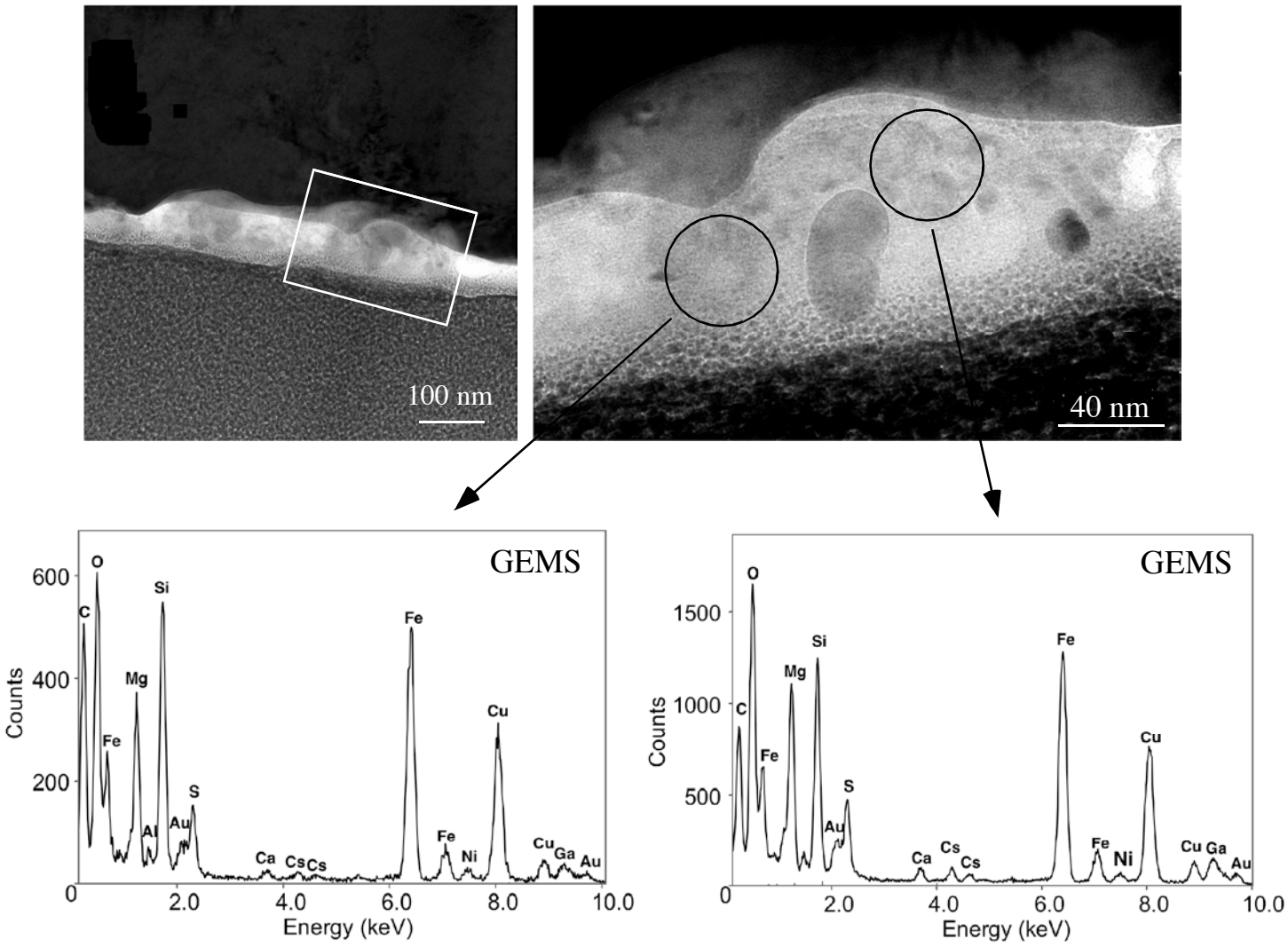
100 nm
40 nm
GEMS
Counts
Energy (keV)
O
C
Fe
Mg
Si
Al
Au
S
Ca
Cs
Cs
Fe
Ni
Cu
Cu
Ga
Au
GEMS
Counts
Energy (keV)
O
C
Fe
Mg
Si
Au
S
Ca
Cs
Cs
Fe
Ni
Cu
Cu
Ga
Au

Figure 15